# Astrocytes Modulate Neural Network Activity by Ca$^{2+}$-Dependent Uptake of Extracellular K$^+$

**Fushun Wang**[1,*], **Nathan A. Smith**[1,*], **Qiwu Xu**[1], **Takumi Fujita**[1], **Akemichi Baba**[2], **Toshio Matsuda**[3], **Takahiro Takano**[1], **Lane Bekar**[1], and **Maiken Nedergaard**[1,†]

[1]Division of Glia Disease and Therapeutics, Center for Translational Neuromedicine, Department of Neurosurgery, University of Rochester Medical School, Rochester, NY 14640, USA

[2]School of Pharmacy, Hyogo University of Health Sciences, Kobe, Hyogo 650-8530, Japan

[3]Graduate School of Pharmaceutical Sciences, Osaka University, Suita, Osaka 565-0871, Japan

## Abstract

Astrocytes are electrically nonexcitable cells that display increases in cytosolic calcium ion (Ca$^{2+}$) in response to various neurotransmitters and neuromodulators. However, the physiological role of astrocytic Ca$^{2+}$ signaling remains controversial. We show here that astrocytic Ca$^{2+}$ signaling ex vivo and in vivo stimulated the Na$^+$,K$^+$-ATPase (Na$^+$- and K$^+$-dependent adenosine triphosphatase), leading to a transient decrease in the extracellular potassium ion (K$^+$) concentration. This in turn led to neuronal hyperpolarization and suppressed baseline excitatory synaptic activity, detected as a reduced frequency of excitatory postsynaptic currents. Synaptic failures decreased in parallel, leading to an increase in synaptic fidelity. The net result was that astrocytes, through active uptake of K$^+$, improved the signal-to-noise ratio of synaptic transmission. Active control of the extracellular K$^+$ concentration thus provides astrocytes with a simple yet powerful mechanism to rapidly modulate network activity.

[†]To whom correspondence should be addressed. nedergaard@urmc.rochester.edu.
[*]These authors contributed equally to this work.

SUPPLEMENTARY MATERIALS
www.sciencesignaling.org/cgi/content/full/5/218/ra26/DC1
Fig. S1. Ouabain-insensitive $^{86}$Rb$^+$ uptake.
Fig. S2. Doxycycline suppresses eGFP expression in cultured astrocytes prepared from MrgA1$^{+/−}$ mice.
Fig. S3. GPCR-activated increases in $^{86}$Rb$^+$ uptake require increases in cytosolic Ca$^{2+}$ in cultured astrocytes.
Fig. S4. Comparison of $^{86}$Rb$^+$ uptake in rat versus mouse and rat cortical versus hippocampal astrocytes.
Fig. S5. Detection of GPCR-activated changes in EPSPs is depth- and [K$^+$]$_{Bath}$-dependent.
Fig. S6. GPCR activation triggers a transient minor increase in intra-astrocytic Na$^+$ concentration and a minor decrease in extracellular Ca$^{2+}$ concentration in hippocampal slices.
Fig. S7. Activation of GPCR-induced changes in PKA and PKC activity does not mediate ATP-induced increases in $^{86}$Rb$^+$ uptake in cultured astrocytes.
Fig. S8. Combined recordings of extracellular K$^+$ with mEPSCs or mIPSCs in hippocampal slices.
Fig. S9. Effects of GPCR activation or reduction of bath K$^+$ concentration on extracellular K$^+$, neuronal membrane potential, and evoked EPSP in hippocampal slices.

## INTRODUCTION

Extracellular $K^+$ is a critical determinant of the resting membrane potential and is normally maintained within a range of 3.0 to 4.0 mM (1). Even minor increases in the extracellular $K^+$ concentration can alter the probability of a neuron firing an action potential by affecting $K^+$ channel gating, slowing action potential recovery (2), modulating synaptic transmission (3), or narrowing the gap between resting membrane potential and the threshold for activation of voltage-gated $Na^+$ channels (4). Astrocytes, which function as sinks for the rapid uptake of extracellular $K^+$ (5), have traditionally been regarded as supportive cells of the central nervous system (CNS) whose major housekeeping functions include the maintenance of extracellular $K^+$ homeostasis (6). The highly negative resting membrane potential (~−85 mV), set by basal $Na^+$- and $K^+$-dependent adenosine tri-phosphatase ($Na^+,K^+$-ATPase) activity, and their large number of inwardly rectifying $K^+$ channels drive excess $K^+$ into astrocytes (7, 8). Although inwardly rectifying $K^+$ channels appear to be primarily responsible for $K^+$ homeostasis at rest, the $Na^+,K^+$-ATPase plays the predominant role in normalizing the increase in extracellular $K^+$ that occurs during neural activity (7–11).

Work in tissues outside the CNS has demonstrated that activity of the $Na^+,K^+$-ATPase is regulated by the second messengers $Ca^{2+}$ and adenosine $3',5'$-monophosphate (cAMP) (5, 7). Moreover, the intracellular $Na^+$ concentrations are rate-limiting for $Na^+,K^+$-ATPase activity in many cell types including astrocytes (8, 9). Thus, increases in cytosolic $Na^+$ concentration in astrocytes could potentially lead to increased activity of the $Na^+, K^+$-ATPase and thereby to a decrease in extracellular $K^+$.

The observations that astrocytes propagate $Ca^{2+}$ signals over considerable distances (12), signal to neurons (13, 14), and modulate neural network activity (15, 16) have sparked interest in defining broader roles for astrocytes in more complex CNS function. Although passive astrocytic buffering of excess $K^+$ is well established (17), whether astrocytes actively control resting extracellular $K^+$ concentration by transiently changing the activity of the $Na^+,K^+$-ATPase is unclear. Astrocytic $Ca^{2+}$ transients play a central role in signaling between neurons and glia (18). Thus, we wondered whether activation of Gq-linked heterotrimeric guanosine triphosphate (GTP)–binding protein (G protein)–coupled receptors (GPCRs) could, through production of inositol 1,4,5-trisphosphate ($IP_3$), activation of its receptor ($IP_3R$), and the subsequent increase in cytosolic $Ca^{2+}$, control the astrocytic $Na^+,K^+$-ATPase activity and thereby modulate neuronal excitability by active uptake of $K^+$.

Here, we show that a rise in cytosolic $Ca^{2+}$ triggers an increase in ouabain-sensitive $K^+$ uptake in cultured astrocytes and a transient decrease in extracellular $K^+$ in hippocampal slices. $Ca^{2+}$-mediated $K^+$ uptake into astrocytes was primarily driven by $Na^+$ influx mediated by astrocyte $Na^+,Ca^{2+}$ exchange. Combined, these findings show that $Ca^{2+}$-dependent activation of the astrocytic $Na^+,K^+$-ATPase through GPCR-activated pathways enables astrocytes to dynamically regulate the extracellular $K^+$ concentration. Because extracellular $K^+$ concentration is a key determinant of neuronal excitability, its active regulation by astrocytes has numerous implications for basic CNS functions.

## RESULTS

### GPCR-activated $Ca^{2+}$ signaling increases $K^+$ uptake in cultured astrocytes

Astrocytes propagate intercellular $Ca^{2+}$ signals through release of adenosine $5'$-triphosphate (ATP) and the consequent activation of purinergic receptors (19, 20); therefore, to evaluate the potential role of astrocytic $Ca^{2+}$ signaling in $K^+$ uptake, we first assessed the role of purinergic receptors on $Na^+,K^+$-ATPase activity by quantifying the ouabain-sensitive fraction of rubidium-86 uptake ($^{86}Rb^+$; used as a $K^+$ analog) (9, 10). ATP stimulated an

increase in ouabain-sensitive $^{86}Rb^+$ uptake averaging $35.6 \pm 7.1\%$ ($n = 27$) in cultured cortical rat astrocytes (Fig. 1A) as well as an increase in cytosolic $Ca^{2+}$. Similarly, uridine 5′-triphosphate (UTP, a P2Y2 and P2Y4 receptor agonist) and 2-methylthioadenosine 5′-diphosphate (2MeSADP, a P2Y1 receptor agonist) increased not only cytosolic $Ca^{2+}$ but also ouabain-sensitive $^{86}Rb^+$ uptake by $24.1 \pm 3.6\%$ ($n = 39$) and $10.7 \pm 3.9\%$ ($n = 8$), respectively (Fig. 1A). Exposure to the protease-activated receptor-1 (PAR1)–selective agonist Thr-Phe-Leu-Leu-Arg-NH$_2$ (TFLLR-NH$_2$) or to prostaglandin E$_2$ (PGE$_2$) also increased cytosolic $Ca^{2+}$ and $K^+$ uptake, whereas the metabotropic glutamate receptor (mGluR) agonist $trans$-(1$S$,3$R$)-1-amino-1,3-cyclopentanedicarboxylic acid ($t$-ACPD) and the P1R agonist adenosine had no effect (Fig. 1A). The ouabain-insensitive fraction of $^{86}Rb^+$ uptake was not altered by GPCR-activated pathways (fig. S1), indicating that other $K^+$ uptake pathways, such as channel-mediated $K^+$ influx, were not affected by changes in cytosolic $Ca^{2+}$.

We prepared astrocyte cultures from transgenic mice expressing an exogenous Gq-coupled receptor (MrgA1) under the control of the inducible human glial fibrillary acidic protein (hGFAP) promoter (21) to further evaluate the $Ca^{2+}$ dependency of GPCR-activated $K^+$ uptake (fig. S2). The MrgA1 agonist peptide Phe-Met-Arg-Phe amide (FMRF) increased intracellular $Ca^{2+}$ and $^{86}Rb^+$ uptake in MrgA1$^{+/-}$ astrocytes (Fig. 1A). $^{86}Rb^+$ uptake increased as a linear function of $Ca^{2+}$ concentration regardless of the ligand used (Fig. 1B, left, $r^2 = 0.94$). Moreover, pretreatment with the endoplasmic reticulum (ER) $Ca^{2+}$ pump inhibitor cyclopiazonic acid (CPA) blocked GPCR-activated increases in cytosolic $Ca^{2+}$ and in ouabain-sensitive $^{86}Rb^+$ uptake as well as nonstimulated ouabain-sensitive $^{86}Rb^+$ uptake (Fig. 1B, right, and fig. S3). In contrast to astrocyte cultures, neuronal cultures failed to show increases in $^{86}Rb^+$ uptake in response to activation of GPCR pathways. 2MeSADP and glutamate reduced $^{86}Rb^+$ uptake in neurons despite triggering increases in cytosolic $Ca^{2+}$ (Fig. 1C). Thus, increases in the cytosolic $Ca^{2+}$ concentration selectively increased $Na^+,K^+$-ATPase activity in astrocytic, but not neuronal cultures (compare Fig. 1, B and D). Whereas these experiments were performed in neo-cortical cultures, UTP-induced $K^+$ uptake appeared to be comparable in astrocytic cultures prepared from hippocampus or cortex from either rat or mouse pups (fig. S4).

To determine whether cytosolic $Ca^{2+}$ increased $Na^+,K^+$-ATPase activity independently of GPCR activation, we exposed astrocytic cultures to increasing concentrations of the $Ca^{2+}$ ionophore ionomycin (22). Ionomycin elicited a dose-dependent increase of ouabain-sensitive $^{86}Rb^+$ uptake and $Ca^{2+}$ responses in astrocyte cultures at 0.05 µM (Fig. 1E). Ionomycin also increased cytosolic $Ca^{2+}$ in neuronal cultures; however, in neuronal cultures, it did not increase $^{86}Rb^+$ uptake (Fig. 1F). Thus, we concluded that increased cytosolic $Ca^{2+}$ can stimulate $Na^+,K^+$-ATPase activity in astrocytes, but not neurons.

## GPCR-mediated astrocytic $Ca^{2+}$ signals decrease extracellular $K^+$ in hippocampal slices

We next investigated whether GPCR-mediated increases in astrocytic $Ca^{2+}$ could regulate extracellular $K^+$. We loaded hippocampal slices with the $Ca^{2+}$ indicator rhod-2 AM (rhod-2 acetoxymethyl ester) to assess GPCR-activated increases in $Ca^{2+}$ and confirmed that FMRF induced robust increases in rhod-2 signal in MrgA1$^{+/-}$ mice, but not in MrgA1$^{-/-}$ littermates (Fig. 2A). To determine whether GPCR-activated decreases in the extracellular $K^+$ concentration were secondary to an increase in astrocyte cytosolic $Ca^{2+}$ concentration, we used mice in which astrocytes are unable to mobilize intracellular $Ca^{2+}$ stores as a consequence of global deletion of IP$_3$R2 (IP$_3$R2$^{-/-}$ mice) (23, 24). Application of ATP, UTP, or TFLLR-NH$_2$ increased cytosolic $Ca^{2+}$ in slices from wild-type (IP$_3$R2$^{+/+}$) mice, whereas, consistent with previous studies (21, 24), they failed to do so in IP$_3$R2$^{-/-}$ mice (Fig. 2B). Using $K^+$-sensitive microelectrodes to measure extracellular $K^+$ (25) 80 µm below the surface, we found that in the presence of a bath concentration of 4 mM $K^+$,

exposure to FMRF, ATP, UTP, or TFLLR-NH$_2$ elicited a transient decrease in the extracellular K$^+$ concentration in wild-type mice (Fig. 2, C and D). This decrease in extracellular K$^+$ concentration was markedly attenuated in IP$_3$R2$^{-/-}$ mice (Fig. 2, C and D). For instance, whereas UTP induced a transient decline in extracellular K$^+$ concentration averaging $-0.43 \pm 0.05$ mM ($n = 6$) in slices prepared from wild-type mice, the K$^+$ decline was only $-0.13 \pm 0.08$ mM ($n = 6$) in IP$_3$R2$^{-/-}$ mice. Similarly, the PAR1 agonist TFLLR-NH$_2$ decreased extracellular K$^+$ by $0.33 \pm 0.04$ mM ($n = 8$) in IP$_3$R2$^{+/+}$ mice, but not in IP$_3$R2$^{-/-}$ mice ($0.05 \pm 0.08$ mM, $n = 5$). Thus, experiments in hippocampal slices were consistent with the hypothesis that GPCR-activated increases in astrocyte cytosolic Ca$^{2+}$ lead to decreased extracellular K$^+$. These GPCR-activated decreases in extracellular K$^+$ concentration were not apparent, however, when K$^+$ concentration was recorded <30 μm below the surface of the slice or at a subphysiological bath concentration of K$^+$ (2.5 mM) (fig. S5).

Astrocytic Na$^+$,K$^+$-ATPase activity is stimulated by small increases in extracellular K$^+$, but decreased at subphysiological extracellular K$^+$ concentrations (26, 27). This enables astrocytes to transiently buffer the minor increases in extracellular K$^+$ concentration that occur during neural activity and then slowly release K$^+$ during the period of decreased extracellular K$^+$ that follows (28). We wondered whether the increase in K$^+$ uptake that occurs in response to increases in extracellular K$^+$ concentration depended on cytosolic Ca$^{2+}$ signals in astrocytes. We found that ouabain-sensitive $^{86}$Rb$^+$ uptake increased with increasing extracellular K$^+$ concentrations and that preloading cultured astrocytes with CPA blocked the increase in $^{86}$Rb$^+$ uptake when the extracellular K$^+$ concentration was increased from 2.5 to 5 mM, but not when extracellular K$^+$ was increased to 10 or 20 mM (Fig. 3A). We therefore concluded that astrocytic buffering of modest increases of extracellular K$^+$ is potentiated by cytosolic Ca$^{2+}$ increases, whereas buffering of pathophysiological increases of extracellular K$^+$ (10 mM or higher) is Ca$^{2+}$-independent.

To assess whether Ca$^{2+}$-dependent K$^+$ uptake can contribute to buffering of increases in extracellular K$^+$ in response to more physiological stimuli, we compared high-frequency stimulation (HFS)–induced changes in extracellular K$^+$ in hippocampal slices from IP$_3$R2$^{+/+}$ and IP$_3$R2$^{-/-}$ mice. HFS consistently induced a higher peak increase in extracellular K$^+$ in IP$_3$R2$^{-/-}$ mice. Moreover, the undershoot during the K$^+$ recovery was reduced in IP$_3$R2$^{-/-}$ mice (Fig. 3, B and C), consistent with the lack of Ca$^{2+}$ responses in slices prepared from IP$_3$R2$^{-/-}$ mice (Fig. 3C, left). Thus, we concluded that the ability of astrocytes to mobilize intracellular Ca$^{2+}$ is a determinant of astrocytic K$^+$ uptake in hippocampal slices.

## Na$^+$ influx drives GPCR-mediated increases in K$^+$ uptake

In many cell types, including astrocytes, the intracellular Na$^+$ concentration provides the primary mechanism for regulating Na$^+$,K$^+$-ATPase activity (8, 9), which increases with increasing intracellular Na$^+$ concentrations. For example, glutamate uptake stimulates Na$^+$,K$^+$-ATPase activity by increasing cytosolic Na$^+$ (9). To define the role of cytosolic Na$^+$ in GPCR-activated K$^+$ uptake, we used several approaches to manipulate intra-astrocytic Na$^+$. These included removal of extracellular Na$^+$, application of the Na$^+$ ionophore monensin, inhibition of the Na$^+$,Ca$^{2+}$ exchanger (NCX), and inhibition of store-operated Ca$^{2+}$ channels (SOCs) (Fig. 4). We first assessed whether Na$^+$ was necessary for GPCR-activated K$^+$ uptake. Removal of extracellular Na$^+$ reduced baseline ouabain-sensitive $^{86}$Rb$^+$ uptake and eliminated GPCR-activated increases, supporting the notion that Na$^+$ is required for both baseline and Ca$^{2+}$-induced increases in Na$^+$,K$^+$-ATPase activity (Fig. 4A). One mechanism whereby increases in intracellular Ca$^{2+}$ could increase Na$^+$ availability in astrocytes involves the NCX, which uses the energy stored in the Na$^+$ electrochemical gradient to extrude Ca$^{2+}$ (exchanging three Na$^+$ for one Ca$^{2+}$) (29, 30). We found that the NCX inhibitors SN-6 and SEA0400 (31) decreased TFLLR-NH$_2$–induced $^{86}$Rb$^+$ uptake

(Fig. 4B). Consistent with cytosolic $Na^+$ being rate-limiting for $Na^+,K^+$-ATPase, the $Na^+$ ionophore monensin triggered a dose-dependent increase of $^{86}Rb^+$ uptake in both astrocytic and neuronal cultures (Fig. 4C). Monensin-induced $^{86}Rb^+$ uptake was of larger amplitude than GPCR-activated uptake in astrocytes and severalfold higher in astrocytic than neuronal cultures (compare Figs. 1A and 4C), suggesting that the $Na^+,K^+$-ATPase activity is not maximally activated by GPCR-activated increases in cytosolic $Ca^{2+}$. As previously reported (32), however, monensin also induced $Ca^{2+}$ increases in cultured astrocytes. To dissect the relative contribution of $Na^+$ influx versus $Ca^{2+}$ increases, we attenuated monensin-induced cytosolic $Ca^{2+}$ increases by preloading them with CPA. CPA reduced monensin-induced $^{86}Rb^+$ uptake (by ~30%), indicating that the predominant action of monensin on $Na^+,K^+$-ATPase activity involves the increase in intracellular $Na^+$ rather than that in $Ca^{2+}$. The NCX inhibitors SN-6 and SEA0400 reduced $^{86}Rb^+$ uptake without decreasing the intracellular $Ca^{2+}$ concentration, suggesting that SN-6 and SEA0400 not only inhibit NCX, but may have other effects, or that the NCX may contribute to $^{86}Rb^+$ uptake through some alternative mechanism. Thus, this analysis indicates that the NCX contributes to GPCR-activated increases in ouabain-sensitive $^{86}Rb^+$ uptake and that it is possible to bypass the NCX by directly increasing intracellular $Na^+$ concentration (Fig. 4D).

Depletion of intracellular $Ca^{2+}$ stores during $Ca^{2+}$ signaling in astrocytes has previously been shown to result in opening of SOCs (33). These $Ca^{2+}$ channels, which in astrocytes include transient receptor potential C1 (TRPC1) channels (34), represent a major pathway for $Ca^{2+}$ entry in nonexcitable cells (35, 36). Indeed, using $Ca^{2+}$-sensitive micro-electrodes, we found that GPCR-activated $Ca^{2+}$ signaling in astrocytes induced a transient decrease in extracellular $Ca^{2+}$ averaging ~0.1 mM, from a resting concentration ranging from 1.2 to 1.4 mM (fig. S6) (33, 37). SKF96365, a nonspecific inhibitor of TRPC1 (38), shortened GPCR-activated $Ca^{2+}$ increases and suppressed $^{86}Rb^+$ uptake (Fig. 4, E and F).

We used $K^+$-sensitive microelectrodes to determine whether the NCX plays a role in GPCR-mediated $K^+$ uptake in hippocampal slices. $Na^+$ in the bath was replaced with *N*-methyl-D-glucamine ($NMDG^+$). $Na^+$ suppressed GPCR-activated decreases in extracellular $K^+$ (Fig. 4, G and H). Moreover, the NCX inhibitors SN-6 and SEA0400 attenuated the transient decline in extracellular $K^+$ triggered by TFLLR-$NH_2$ (Fig. 4, G and H). The TRPC1 inhibitor SKF96365 also attenuated GPCR-activated decreases in extracellular $K^+$ and suppressed TFLLR-$NH_2$–induced $Ca^{2+}$ increases (Fig. 4I). Together, these observations suggest that high cytosolic $Ca^{2+}$ activates the NCX. In turn, the inflow of $Na^+$ ions activates the $Na^+,K^+$-ATPase, resulting in a transient decrease in extracellular $K^+$ (Fig. 4J).

Support for this model was obtained by an analysis of cytosolic $Na^+$ concentration in cultured astrocytes. Astrocytes loaded with the fluorescent $Na^+$ indicator sodium-binding benzofuran isophthalate (SBFI) (26, 27) showed a small increase in SBFI fluorescence when exposed to either ATP or FMRF in hippocampal slices from MrgA1$^{+/-}$ mice ($n = 5$; $P < 0.01$ compared to before, *t* test) that paralleled in increase in cytosolic $Ca^{2+}$ (fig. S6). Thus, several lines of analysis show that increases in cytosolic $Na^+$ may be a prerequisite for GPCR-activated reductions in extracellular $K^+$.

$Na^+,K^+$-ATPase activity is regulated by both protein kinase C (PKC)–and PKA-mediated phosphorylation in a broad range of cell types (39, 40). However, an analysis of cultured astrocytes showed that pharmacological activation or inhibition of PKA or PKC activity consistently suppressed GPCR-activated $^{86}Rb^+$ uptake (fig. S7). This suggests that PKC- or PKA-mediated modulation of the $Na^+,K^+$-ATPase activity is optimal under resting in cultured astrocytes. However, kinase regulation of the $Na^+,K^+$-ATPase activity is complex and dependent on the ambient concentrations of cytosolic $Ca^{2+}$ and $Na^+$ (39). Thus, we

cannot eliminate the possibility that kinase modulation regulates the activity of the $Na^+,K^+$-ATPase activity in vivo.

## Astrocytic $Ca^{2+}$ signaling suppresses basal excitatory synaptic activity

Given that the $Na^+,K^+$-ATPase activity in astrocytes is modulated by changes in the cytosolic $Ca^{2+}$ concentration, we wondered whether astrocytes might modulate synaptic activity through dynamic changes in extracellular $K^+$. Although several studies have addressed the role of pathological increases in extracellular $K^+$ on synaptic activity (17, 41, 42), the effects of lowering extracellular $K^+$ are less clear. We achieved reductions in extracellular $K^+$ by either exposing hippocampal slices from $MrgA1^{+/-}$ mice to FMRF for 1 min (Fig. 5, A and B and E and F, and fig. S8) or reducing bath $K^+$ from 4 to 2 mM for 2 min (Fig. 5, C and D and G and H, and fig. S8). Extracellular $K^+$ fell from $3.81 \pm 0.07$ to $3.14 \pm 0.06$ mM ($n = 13$) when bath $K^+$ was lowered from 4 to 2 mM, similar to the drop in extracellular $K^+$ evoked by GPCR-activated astrocytic $Ca^{2+}$ signaling (see Figs. 2D and 4I). CA1 hippocampal neurons typically underwent a small hyperpolarization in response to decreasing the bath extracellular $K^+$ concentration ($-3.44 \pm 0.37$ mV, $n = 13$). Similarly, FMRF triggered a small hyperpolarization in CA1 neurons in $MrgA1^{+/-}$ mice ($-1.78 \pm 0.33$ mV, $n = 6$), whereas it did not affect the membrane potential ($0.22 \pm 0.12$ mV, $n = 6$) of CA1 neurons in littermates ($MrgA1^{-/-}$). Thus, $Ca^{2+}$ signaling in hippocampal astrocytes is linked to a minor hyperpolarization of the membrane potential of CA1 neurons.

Neuronal hyperpolarization was associated with a decrease in the frequency of miniature excitatory postsynaptic currents (mEPSCs) (Fig. 5, A to D). The frequency of mEPSCs fell from $1.37 \pm 0.17$ to $0.80 \pm 0.10$ Hz during FMRF application ($n = 9$, Fig. 5B) and from $1.61 \pm 0.27$ to $0.68 \pm 0.13$ Hz when bath $K^+$ concentration was lowered to 2 mM $K^+$ ($n = 8$, Fig. 5D). Moreover, repolarization of mEPSCs occurred more rapidly when the extracellular $K^+$ concentration was reduced (Fig. 5, B and D), likely reflecting the increase in $K^+$ driving force. mEPSC recovery (assessed as the time constant of decay, $\tau$) fell from $97.2 \pm 13.6$ to $66.5 \pm 7.9$ ms during FMRF application ($n = 9$, Fig. 5B) and from $95.4 \pm 16.6$ to $63.6 \pm 14.5$ ms when bath $K^+$ concentration was lowered to 2 mM $K^+$ ($n = 8$, Fig. 5D). Lowering of extracellular $K^+$ may therefore suppress excitatory synaptic activity by reducing both the probability of glutamate release from presynaptic terminals and the duration of the depolarization of the postsynaptic membrane. In contrast, miniature inhibitory postsynaptic currents (mIPSCs) were largely unaffected by lowering of extracellular $K^+$ (Fig. 5, E to H). mIPSC frequency before and after FMRF application was $0.56 \pm 0.08$ to $0.45 \pm 0.10$ Hz ($n = 7$, Fig. 5, E to F) and $0.66 \pm 0.03$ to $0.62 \pm 0.06$ Hz ($n = 7$) before and after reduction of bath $K^+$ concentration from 4 to 2 mM (Fig. 5, G and H). Moreover, lowering of bath $K^+$ concentration or exposure to FMRF had no effects on mIPSC recovery ($\tau$) (Fig. 5H). The lack of effects with manipulation of extracellular $K^+$ on inhibitory transmission has been previously reported (43, 44). Postsynaptically, the IPSCs are mediated by a transient increase in $Cl^-$ conductance, which is insensitive to minor changes in extracellular $K^+$ (45). Moreover, presynaptically, inhibitory neurons express Kv3 potassium channels in their terminals. Kv3 channels are inactive at resting membrane potential, and their open probability is not altered in response to minor voltage changes (46–48). Thus, the net effect of lowering extracellular $K^+$ is a selective reduction of spontaneous excitatory transmission, which can be considered a suppression of background synaptic noise.

## Astrocytic $Ca^{2+}$ signaling enhances the signal-to-noise ratio of excitatory synaptic transmission

Given that astrocytic $Ca^{2+}$ signaling decreased basal excitatory activity, we next asked what effect it had on synaptic transmission. We used evoked excitatory postsynaptic potentials (eEPSPs) as signal and spontaneous EPSPs (sEPSPs) as a measurement of background

afferent synaptic transmission (noise) by obtaining whole-cell recordings from CA1 hippocampal neurons while stimulating the Schaeffer collaterals with a stimulation electrode placed in the stratum radiatum (stimulation interval, 2 s) (Fig. 6A). FMRF decreased the frequency of sEPSPs in slices from $MrgA1^{+/-}$ mice, but not the amplitude of eEPSP concurrently with a transient decrease in the extracellular $K^+$ concentration (Fig. 6A). In contrast, FMRF failed to alter either the frequency of sEPSPs, the amplitude of the eEPSP, or the concentration of extracellular $K^+$ in $MrgA1^{-/-}$ littermates (Fig. 6A). To more broadly assess the effect of astrocytic $Ca^{2+}$ signaling on excitatory synaptic transmission, we next exposed slices to an array of GPCR agonists, including ATP, UTP, 2MeSADP, and TFLLR-$NH_2$. Combined whole-cell recordings of CA1 neurons with measurements of extracellular $K^+$ showed that GPCR-activated pathways triggered a transient neuronal hyperpolarization (fig. S9) concomitantly with a decrease in the frequency of sEPSPs (Fig. 6B). The frequency of sEPSPs decreased as a direct function of the reduction of extracellular $K^+$ (Fig. 6B). To address the effect of GPCR-activated $Ca^{2+}$ signaling in astrocytes on hippocampal network function, we calculated the signal-to-noise ratio (SNR): eEPSPs were taken as signal and sEPSPs were taken as noise (Fig. 6C). The integrated area of all the eEPSPs was divided by the integrated area of all the sEPSPs within the same time period (49–51). We found that the SNR increased in response to GPCR-activated $Ca^{2+}$ signaling in astrocytes, primarily a reflection of the fact that the eEPSP amplitude was insensitive to reductions in the extracellular $K^+$ concentration (fig. S9), whereas the frequency of sEPSPs decreased in response to astrocytic $K^+$ uptake (Fig. 6B).

We next asked whether a reduction in bath $K^+$ concentration was sufficient to reproduce the effects of GPCR-activated astrocytic $Ca^{2+}$ signaling on excitatory synaptic transmission. We first assessed the impact of minor transient reductions of bath $K^+$ on sEPSPs and eEPSPs. In these experiments, whole-cell recordings of CA1 pyramidal neurons were combined with measurements of extracellular $K^+$, because the actual changes in interstitial $K^+$ concentration were of smaller amplitude than in the bath solution (fig. S9A). For example, reducing bath $K^+$ concentration from 4 to 2 mM for 2 min only lowered interstitial $K^+$ concentration by ~0.6 mM (from $3.84 \pm 0.06$ to $3.24 \pm 0.06$ mM, $n = 5$) (fig. S9D). CA1 neurons typically exhibited a minor hyperpolarization in response to lowering the extracellular $K^+$ concentration, and the changes in membrane potential were a linear function of bath $K^+$ concentration ($r^2 = 0.61$, fig. S9E). This hyper-polarization was associated with a suppression of basal excitatory activity detected as a reduction of the frequency of sEPSPs (Fig. 6, D and E). Plotting sEPSP as a function of the decrease in extracellular $K^+$ concentration showed that the frequency (Fig. 6E) of sEPSPs was inversely related to extracellular $K^+$ ($r^2 = 0.36$). Thus, lowering the extracellular $K^+$ concentration reduced spontaneous excitatory activity. Recordings of eEPSP in CA1 neurons showed that eEPSP amplitude was largely insensitive to changes in extracellular $K^+$ over the concentration range studied. Consequently, the ratio of integrated areas for eEPSPs and sEPSPs over the same time period increased as an inverse function of extracellular $K^+$ ($r^2 = 0.54$) (Fig. 6F). We next compared the effect of activation of GPCRs in astrocytes upon sEPSP and eEPSPs in hippocampal slices from $IP_3R2^{-/-}$ mice. UTP (100 $\mu$M) failed to change the frequency of sEPSP (after/before = $1.02 \pm 0.03$, $n = 5$) in slices prepared from $IP_3R2^{-/-}$ mice (Fig. 6G). In contrast, eEPSP amplitude was insensitive to UTP. Thus, mobilization of intracellular $Ca^{2+}$ store in astrocytes was essential for UTP-induced suppression of sEPSPs. In contrast, direct reduction of bath $K^+$ concentration triggered membrane hyperpolarization and a decrease in the frequency of sEPSP in $IP_3R2^{-/-}$ mice (Fig. 6G).

These observations indicate that the reduction in extracellular $K^+$ concentration induced by astrocytic $Ca^{2+}$ signaling leads to an increase in eEPSPs versus sEPSPs.

## Astrocytic Ca$^{2+}$ signaling reduces the frequency of synaptic failures

The stimulation protocol used above for eEPSPs will recruit essentially all fibers in the Schaffer collaterals and may not detect minor modulation of synaptic transmission triggered by decreased extracellular K$^+$ concentration. To investigate the possibility that astrocytic Ca$^{2+}$ signaling enhances the evoked response directly, we used a minimal stimulation protocol (52, 53) in which we placed a glass electrode in the stratum radiatum in hippocampal CA1 and adjusted the stimulus to approximate the threshold for getting synaptic failures (~50%). By stimulation of a small number of Schaffer collaterals (potentially a single fiber), the effects of minor reductions in extracellular K$^+$ on synaptic fidelity can be quantified. At 4 mM extracellular K$^+$, the rate of synaptic failures detected by whole-cell recording from CA1 neurons averaged $0.46 \pm 0.03$ ($n = 33$). FMRF application in MrgA1$^{+/-}$ slices (Fig. 7A) or directly lowering bath K$^+$ concentration of these slices (Fig. 7B) consistently reduced conduction failures (Fig. 7C). No effects were observed on synaptic potency (mean amplitude of successful stimuli) (Fig. 7D), indicating that the decrease in conduction failure was associated with an increase in synaptic efficacy (mean amplitude of all stimuli) (Fig. 7E). Because mGluRs reduce astrocyte-mediated increases in synaptic efficacy (52, 53), we administered FMRF to MrgA1$^{+/-}$ slices in the presence of the mGluR antagonists 6-methyl-2-(phenylethynyl)pyridine hydrochloride (MPEP) (50 μM) and LY367385 (100 μM) and found that synaptic failures still decreased from $0.46 \pm 0.07$ to $0.24 \pm 0.04$ ($n = 6$, $P < 0.01$, paired $t$ test). Similarly, synaptic efficacy increased from $1.02 \pm 0.13$ mV to $1.5 \pm 0.19$ mV ($n = 6$, $P < 0.01$, paired $t$ test), whereas synaptic potency remained unchanged, $1.96 \pm 0.19$ mV to $1.97 \pm 0.08$ mV ($n = 6$, $P = 0.38$). Thus, MPEP and LY367385 did not interfere with suppression of synaptic failures evoked by FMRF-induced astrocytic Ca$^{2+}$ signaling. The minimal stimulation protocol provides a more sensitive dissection of the effect of astrocytic Ca$^{2+}$ signaling on eEPSPs. The net effect of astrocytic activation is therefore a transient increase in circuit SNR.

## GPCR-activated astrocytic Ca$^{2+}$ signaling mediates a decrease in extracellular K$^+$ concentration in vivo

We next assessed the effects of astrocytic Ca$^{2+}$ signaling on extracellular K$^+$ in live adult mice, using topical application of agonists in an open cranial window preparation to trigger astrocytic Ca$^{2+}$ signaling. We used this approach, rather than evoking Ca$^{2+}$ signaling by sensory stimulation, because interpretation of sensory-evoked changes in extracellular K$^+$ concentration is complicated by the direct effect of synaptic activity upon extracellular K$^+$ (17, 42, 54, 55). We first evaluated the efficacy of different agonists in triggering cytosolic Ca$^{2+}$ increases in cortical astrocytes. The exposed cortex was loaded with the Ca$^{2+}$ indicator rhod-2 AM (56–59) and superfused with either ATP (100 μM) in Glt1-eGFP (enhanced green fluorescent protein) reporter mice (60) or FMRF in MrgA1$^{+/-}$ mice (21). Both ATP and FMRF evoked robust increases in cytosolic Ca$^{2+}$ in astrocytes located 100 μm below the pial surface (Fig. 8, A to D). Moreover, extracellular K$^+$ recorded at a depth of ~100 μm exhibited a transient decline in response to either ATP or FMRF superfusion (Fig. 8, E and F). Amplitudes of Ca$^{2+}$ increases ($\Delta F/F$) and reductions in extracellular K$^+$ were similar to those observed in acute slice preparations from mouse pups. Thus, astrocytic Ca$^{2+}$ signaling in live adult mice can also trigger a transient reduction in the extracellular K$^+$ concentration.

## DISCUSSION

We show here that GPCR-mediated Ca$^{2+}$ signaling in astrocytes is linked to an increase in K$^+$ uptake resulting in a transient decrease in the extracellular concentration of K$^+$ (Fig. 1). The average decrease in the extracellular K$^+$ concentration was in the range of 0.3 to 0.6 mM and lasted 20 to 80 s in hippocampal slice preparations as well as in live adult mouse cortex (Figs. 2 and 8). A detailed analysis suggested that the transient increase in astrocytic

$K^+$ uptake was mediated primarily by the $Na^+,K^+$-ATPase (Fig. 4 and fig. S1). The intracellular $Na^+$ concentration has been identified as a factor that limits the rate of $Na^+,K^+$-ATPase activity in astrocytes as in other cell types (8–11). We confirmed this observation and showed that $Ca^{2+}$-mediated activation of the $Na^+,K^+$-ATPase, at least in part, is the result of $Na^+$ influx through the $Na^+,Ca^{2+}$ exchanger, because removal of extracellular $Na^+$ or addition of inhibitors of the $Na^+,Ca^{2+}$ exchanger reduced or eliminated GPCR-activated astrocytic $K^+$ uptake (Fig. 4). In support of the proposed mechanism (Fig. 4J), we found that cytosolic $Na^+$ concentration in hippocampal astrocytes increased slightly in response to activation of GPCR pathways (fig. S7). The classical role of astrocytes is to buffer excess $K^+$ released during synaptic transmission. Previous analyses have shown that astrocytes are specialized for rapid removal of $K^+$, because the astrocytic $Na^+,K^+$-ATPase exhibits an unusual sensitivity to minor increases in extracellular $K^+$ (26, 27). We confirmed these original observation and extended them by showing that $Ca^{2+}$ signaling potentiated $K^+$ uptake in response to modest increases of extracellular $K^+$ (5 mM), but not when $K^+$ is raised to pathological concentrations (10 mM or higher) (Fig. 3). Moreover, we showed that GPCR-activated $Ca^{2+}$ signaling in astrocytes reduces baseline extracellular $K^+$ concentration in slices (Figs. 2D and 4H) and in vivo (Fig. 8). As expected, lowering the extracellular $K^+$ concentration led to a neuronal hyperpolarization averaging −2 to −4 mV. The hyperpolarization was observed in response to direct lowering of bath $K^+$ concentration, or indirectly by stimulating astrocytic $Ca^{2+}$ signaling. As previously described, lowering the extracellular $K^+$ concentration decreased the frequency and the duration of mEPSCs (61, 62) in hippocampal slices, but had little effect on eEPSP amplitude (Figs. 5 and 6) (43, 44). However, when a minimal stimulation protocol was used, we found that astrocytic $Ca^{2+}$ signaling triggered a small but significant decrease in synaptic failures ($P < 0.01$ compared to "Before," Bonferroni-Dunn test, $n = 7$, Fig. 7). Thus, the transient reduction of extracellular $K^+$ evoked by astrocytic $Ca^{2+}$ signaling decreased synaptic noise (concomitant with an increase in synaptic fidelity detected as a decrease in synaptic failures). The net effect was that astrocytic $Ca^{2+}$ signaling improved the SNR of hippocampal neurotransmission. Thus, $Ca^{2+}$-mediated $K^+$ uptake endows astrocytes with a simple yet powerful mechanism for rapid modulation of neural activity. We have observed $Ca^{2+}$-dependent $K^+$ uptake in cortex, hippocampus, and cerebellum, suggesting that this signaling pathway is active in many areas of CNS.

Potassium homeostasis is unquestionably an essential housekeeping duty of astrocytes. The concept of astrocytic "$K^+$ spatial buffering" in which $K^+$ is taken up in regions of high extracellular $K^+$ concentration and released at distant sites was first advanced in a leech CNS preparation (63) and later confirmed in isolated retinal Muller cells (64). It was subsequently established that astrocytic $K^+$ uptake is accomplished through multiple mechanisms (10). One study found that the astrocytic $Na^+,K^+$-ATPase constituted the dominant mechanism for $K^+$ recovery after high-frequency neuronal activity (9), whereas other studies provided evidence suggesting that inwardly rectifying $K^+$ channels play a predominant role in maintenance of resting extracellular $K^+$ concentration and recovery from mild neuronal activity (1, 8, 9). However, the relative importance of the $Na^+,K^+$-ATPase and inward rectifying potassium channels in $K^+$ buffering may exhibit regional differences. For example, the $Na^+,K^+$-ATPase is solely responsible for $K^+$ buffering in rat optic nerve (1), whereas $K^+$ siphoning through inwardly rectifying K channels is important in the retina (64). Thus, additional studies are needed to definitively establish whether the mechanism described here is active in regions outside the hippocampus and cortex.

Although our in vitro analysis indicates that the $Na^+,Ca^{2+}$ exchanger, at least in part, provides $Na^+$ ions to fuel the $Na^+,K^+$-ATPase, the catalytic activity of the $Na^+,K^+$-ATPase is regulated by multiple pathways, including phosphorylation of the catalytic α subunit (65). The astrocytic $Na^+,K^+$-ATPase is also activated by minor increases in extracellular $K^+$

concentration, consistent with the role in astrocytic buffering of excess $K^+$ released during neuronal activity (26, 27). Additional studies are required to establish the relative contribution of the many potential regulatory pathways that determine the activity of the $Na^+,K^+$-ATPase.

Through strict regulation of the extracellular $K^+$ concentration, astrocytes exert powerful control over the membrane potential of both excitatory and inhibitory synapses. Why then, do astrocyte-mediated $Ca^{2+}$-dependent decreases in extracellular $K^+$ modulate excitatory and not inhibitory transmission? This question can be addressed by considering the differences between these two modes of synaptic communication in light of the mechanisms by which lowering the extracellular $K^+$ concentration modulates synaptic transmission: (i) the decay kinetics of the mEPSC versus those of the mIPSC, (ii) the voltage dependence of presynaptic ion channels in excitatory and inhibitory nerve terminals, and (iii) the probability of axonal conductance failure. First, the shortening of mEPSCs we observed in response to lowering of extracellular $K^+$ has been reported before (66) and likely reflects that cation currents drive excitatory currents. Low $K^+$ will tend to shorten mEPSCs, because the decay of mEPSCs in part is driven by the outward $K^+$ current. Simply, a reduction of extracellular $K^+$ will increase the driving force for the outward $K^+$ currents and therefore shorten the decay of mEPSCs (61). In contrast, the decay of mIPSCs is primarily mediated by desensitization of $GABA_A$ ($\gamma$-aminobutyric acid type A) receptors (45) and is therefore insensitive to minor decreases in the extracellular $K^+$ concentration. The decrease in the frequency of mEPSCs, but not that of mIPSCs, in response to low extracellular $K^+$ likely might result from differences in the properties of potassium channels found in nerve terminals of excitatory (67) versus inhibitory neurons (47, 48). Potassium channels in excitatory neurons exhibit rapid depolarization-induced inactivation with slow reactivation kinetics upon repolarization (67). In contrast, potassium channels in inhibitory neurons are activated only at relatively depolarized potentials, and their open probability is not altered in response to neuronal hyperpolarization (68). The net result of astrocytic $Ca^{2+}$-mediated $K^+$ uptake is therefore a decrease in the frequency and duration of mEPSCs, whereas mIPSCs are largely insensitive. Lastly, the increase in synaptic fidelity associated with low extracellular $K^+$ is most likely a consequence of the direct effect of extracellular $K^+$ on axonal conduction (44). High extracellular $K^+$ concentration increases the rate of action potential conduction failure in various types of neurons (44, 69), an observation that has been attributed to the slowing of $Na^+$ channel recovery from inactivation. Conversely, a decrease in $K^+$ concentration will hasten $Na^+$ channel recovery and improve action potential conduction reliability. The consequence of the transient lowering of extracellular $K^+$ concentration during GPCR-activated astrocytic $Ca^{2+}$ signaling is thereby a selective reduction in mEPSCs (background noise) concomitant with enhancement of conduction reliability (signal). Thus, astrocytic $Ca^{2+}$ signaling will enhance network SNR and thereby improve information processing. The ability of astrocytes to decrease extracellular $K^+$ concentration provides an elegantly simple and powerful means for rapid astrocytic modulation of network activity. Previous studies on neuroglial signaling have primarily focused on gliotransmitters rather than measurements of extracellular $K^+$ or neuronal membrane potential. In addition, recordings in this study were obtained in neurons located deeper than 80 $\mu$m from the surface of the slice. We found that GPCR-activated changes in $K^+$ were of smaller amplitude near the surface of the slice, where the bath solution rapidly buffers the response (fig. S5). Lastly, many previous studies of neuroglial signaling used bath solution containing 2.5 mM $K^+$, an artificially low concentration of $K^+$, given extracellular $K^+$ in vivo is in the range of 3.0 to 4.0 mM in rat brain cortex (58). GPCR-activated astrocytic modulation of EPSPs was not detectable when we used a bath solution containing 2.5 mM $K^+$ (fig. S5). Thus, it is possible that these and other experimental details have attenuated the effects of $Ca^{2+}$-dependent $K^+$ uptake in astrocytes and obscured this mechanism of neuroglial signaling.

Our findings support the existence of a previously unappreciated mechanism by which astrocytes can modulate neuronal function. Hence, astrocytic control of extracellular $K^+$ concentration may, at least in part, be responsible for effects on neural networks that hitherto have been ascribed to $Ca^{2+}$-dependent release of gliotransmitters. Neuromodulators, many of which potently increase astrocytic $Ca^{2+}$ signals (59), are likewise well suited to mediate large-scale network modulation through astrocytic control of extracellular $K^+$.

## MATERIALS AND METHODS

### Cultures

Cultured neocortical astrocytes were prepared from 1- to 2-day-old Wistar rat pups (Taconic Farms Inc.) or C57BL/6 mouse pups (Taconic Farms) as previously described (70). Briefly, cerebral cortices were dissected and meninges were removed. The tissue was washed three times in Hank's balanced salt solution without $Ca^{2+}$. Once washed, the tissue was triturated, filtered through 70-$\mu$m nylon mesh, and centrifuged. The pellet was resuspended in 10% fetal bovine serum in Dulbecco's modified Eagle's medium (DMEM)/F12 containing penicillin (100 IU ml$^{-1}$) and streptomycin (100 $\mu$g ml$^{-1}$) and transferred to culture flasks. Cells were maintained at 37°C in an incubator containing humidified air and 5% $CO_2$. Medium was changed after 24 hours and twice a week thereafter. More than 95% of the cells stained positive for GFAP. When the monolayers became confluent, they were rinsed two times in Hank's balanced salt solution without $Ca^{2+}$, suspended in 0.05% trypsin-containing solution for 1 min, resuspended in DMEM/F12, centrifuged to remove trypsin, and then plated in 24-well plates. Experiments were performed when the cells were 95% confluent.

A comparison of $^{86}Rb^+$ uptake in astrocytic cultures prepared from rat and mouse astrocytes as well as cultures of rat cortical and hippocampal astrocytes showed no differences in basal or GPCR-activated $^{86}Rb^+$ uptake, except for a higher sensitivity to ouabain of cultures prepared from rat (fig. S4). Unless otherwise noted, rat neocortical cultures were used for $^{86}Rb^+$ uptake experiments. Cultured neocortical neurons were prepared from 1- to 3-day-old Wistar rat pups as previously described (42), with slight modification. Briefly, cerebral cortices were dissected and meninges were removed. The tissues were minced and then suspended in Hibernate A solution minus calcium (BrainBits, LLC) containing papain (Worthington) at 37°C for 30 min. The suspension was then triturated with a 9-inch siliconized pipette. The cell suspension was then separated by density gradient centrifugation. The neuronal cells were then seeded onto poly-D-lysine–coated 24-well plates and maintained in Neurobasal A medium (Invitrogen) with 0.5 ml of B27, 0.5 mM GlutaMAX, gentamycin (10 $\mu$g ml$^{-1}$), and human fibroblast growth factor 2 (FGF2) (5 ng ml$^{-1}$) at 37°C in an incubator containing humidified air and 5% $CO_2$. Immunohistochemistry showed that more than 90% cells in the cultures [identified by DAPI (4′,6-diamidino-2-phenylindole)–stained nuclei] were MAP2-positive. Neuronal cultures were used 8 days after plating. All animal experiments were conducted in accordance with the guidelines of the Animal Care and Use Committee of the University of Rochester.

### $^{86}Rb^+$ uptake assay and $Ca^{2+}$ imaging of cultured cells

On the day of the experiment, culture medium was replaced with oxygenated artificial cerebrospinal fluid (aCSF) (pH 7.4, osmolarity = 310 mosM). After a 30-min recovery period, the cells were incubated for 10 min in the presence or absence of ouabain. The potassium analog $^{86}Rb^+$ was added to each of the 24 wells for 15 min (1 $\mu$Ci, Perkin Elmer). The reaction was stopped by placing the cells on ice and washing them three times with ice-cold aCSF. The remaining aCSF was removed, the cells were lysed with NaOH (100 $\mu$l of 0.5 N), and $^{86}Rb^+$ uptake was quantified by liquid scintillation counting (Beckman Coulter). Ouabain-sensitive $^{86}Rb^+$ uptake was calculated by subtracting $^{86}Rb^+$ uptake during the same

conditions, but in the presence of ouabain (1 mM). For experiments where 5, 10, and 20 mM $K^+$ were used to stimulate $^{86}Rb^+$ uptake, the $^{86}Rb^+$ concentration was increased proportionally with $K^+$ concentration.

For imaging of GPCR-activated increases in $Ca^{2+}$, cultures were loaded with rhod-2 AM (4.5 $\mu$M), and rhod-2 signal was visualized by confocal microscopy (FV500, Olympus) every 3 s before and after application of agonists. The peak fluorescence intensity was calculated as percentage of baseline intensity before stimulation ($\Delta F/F$). Pharmacological agents used in cultures included adenosine (100 $\mu$M), ATP (100 $\mu$M), CPA (20 $\mu$M), glutamate (100 $\mu$M), H89 (10 $\mu$M), ionomycin (0.01 to 0.05 $\mu$M), monensin (5 nM to 3 $\mu$M), $t$-ACPD (100 $\mu$M), 2MeSADP (100 $\mu$M, Tocris), $N^6$,2′-$O$-dibutyryladenosine cAMP (DBcAMP, 1 mM), PGE$_2$ (20 $\mu$M, Tocris), ouabain (1 mM), FMRF (15 $\mu$M), rhod-2 AM (4.5 $\mu$M, Invitrogen), phorbol 12-myristate 13-acetate (PMA, 1 $\mu$M), SEA0400 (10 $\mu$M, synthesized by Taisyo Pharmaceutical Co. Ltd.), potassium chloride (KCl, 5, 10, 20 mM), 1-[2-(4-methoxyphenyl)-2-[3-(4-methoxyphenyl)propoxy]ethyl]imidazole (SKF96365, 25 $\mu$M), (2-[[4-[(4nitrophenyl) methoxy]phenyl]methyl]-4-thiazolidinecarboxylic acid ethyl ester (SN6, 10 $\mu$M, Tocris), staurosporine (2 $\mu$M), UTP (100 $\mu$M), TFLLR-NH$_2$ (30 $\mu$M, Tocris), MPEP (50 $\mu$M), LY367385 (100 $\mu$M), and DL-$threo$-β-benzyloxyaspartic acid (TBOA, 100 $\mu$M, Tocris). All chemicals were from Sigma unless otherwise noted.

## Fabrication and calibration of $K^+$- and $Ca^{2+}$-sensitive microelectrodes

To detect $K^+$ changes in the extracellular space, we fabricated ion-sensitive microelectrodes from double-barreled pipette glass (PB150F-6, WPI) pulled to a tip of <3 $\mu$m with a puller (Sutter P-97). Pipettes were silanized by dimethylsilane (Fluka, Sigma) loaded with a 100- to 150-$\mu$m column of valinomycin-based $K^+$ ion-exchange resin (Potassium Ionophore 1-Cocktail B, Fluka, Sigma), and backfilled with 150 mM KCl. The reference barrel was filled with Hepes-buffered 150 mM NaCl solution (pH 7.4) (25, 71, 72). The pipette was connected to headstages of an Axoprobe 700B amplifier (Axon Instruments). Electrodes were calibrated in 1 to 6 mM $K^+$ in aCSF before and after experiments. The recording pipette was located ~100 $\mu$m below the surface of the slice. The electrodes used in experiments typically displayed voltage responses of 5 to 6 mV per millimolar increase in $K^+$ concentrations in the concentration range studied. In selected experiments, single-barrel pipettes were used in combination with a reference electrode located ~10 $\mu$m away.

Fabrication and use of $Ca^{2+}$-sensitive microelectrodes was similar to that of $K^+$-sensitive microelectrodes, except that the $Ca^{2+}$ ion-exchange resin (Calcium Ionophore 1-Cocktail A, Fluka, Sigma) was used and the pipettes were backfilled with 100 mM CaCl$_2$ (73).

## Slice preparation, electrophysiology, and $Ca^{2+}$ and $Na^+$ imaging

Unless otherwise noted, 15- to 21-day-old C57BL/6 (Charles River), MrgA1$^{+/-}$, MrgA1$^{-/-}$, IP$_3$R2$^{+/+}$, and IP$_3$R2$^{-/-}$ (21, 24) pups were used for preparation of hippocampal slices as previously described (74). The pups were anesthetized with isoflurane in a closed chamber (1.5%) and decapitated. The brains were rapidly removed and immersed in ice-cold cutting solution that contained 230 mM sucrose, 2.5 mM KCl, 0.5 mM CaCl$_2$, 10 mM MgCl$_2$, 26 mM NaHCO$_3$, 1.25 mM NaH$_2$PO$_4$, and 10 mM glucose (pH 7.2 to 7.4). Coronal slices (400 $\mu$m) were cut with a vibratome (Vibratome Company) and transferred to oxygenated aCSF that contained 126 mM NaCl, 4 mM KCl, 2 mM CaCl$_2$, 1 mM MgCl$_2$, 26 mM NaHCO$_3$, 1.25 mM NaH$_2$PO$_4$, and 10 mM glucose (pH 7.2 to 7.4, osmolarity = 310 mosM). Slices were incubated in aCSF for 1 to 5 hours at room temperature before recording. Experiments were performed at room temperature (21° to 23°C). During the recordings, the slices were placed in a perfusion chamber and superfused with aCSF gassed with 5% CO$_2$ and 95% O$_2$

at room temperature. Cells were visualized with a 40× water-immersion objective and differential inference contrast (DIC) optics (BX51 upright microscope, Olympus Optical).

Patch electrodes were fabricated from filament thin-wall glass (World Precision Instruments) on a vertical puller; the resistance of the pipette was about 6 to 9 megohms with intracellular pipette solution added. Membrane potentials were recorded under current clamp ($I = 0$) with an Axopatch MultiClamp 700B amplifier (Axon Instruments). The pipette solution contained 140 mM K-gluconate, 5 mM Na-phosphocreatine, 2 mM $MgCl_2$, 10 mM Hepes, 4 mM Mg-ATP, and 0.3 mM Na-GTP (pH adjusted to 7.2 with KOH). With these solutions, the IPSCs reversed at −70 mV, and EPSCs reversed at about 0 mV. The junction potential between the patch pipette and the bath solution was zeroed before forming a gigaseal. Patches with seal resistances of less than 1 gigohm were rejected. Data were low pass–filtered at 2 kHz and digitized at 10 kHz with a Digidata 1440 interface controlled by pClamp Software (Molecular Devices).

In experiments recording GPCR-activated changes in $K^+$ or EPSCs, agonists were delivered by superperfusion for a period of 1 min unless otherwise noted. mEPSCs were isolated by adding 0.5 µM tetrodotoxin (TTX) and bicuculline methylchloride (50 µM) to the bath solution and maintaining a holding potential of −70 mV. Miniature IPSCs were isolated with 0.5 µM TTX, CNQX (6-cyano-7-nitroquinoxaline-2,3-dione) (25 µM), and APV (D,L-2-amino-5-phosphonovaleric acid) (50 µM) and a holding potential of −50 mV. HFS was delivered as a train of 300 square pulses (200 µs, 50 to 100 µA) at 100 Hz applied in the stratum radiatum. Minimal stimulation was used to activate single or few presynaptic fibers (52, 53). Briefly, a glass pipette filled with aCSF (3 µm tip) was positioned in the stratum radiatum so that 100-µs current pulse evoked postsynaptic potentials in a patched CA1 neuron. The stimulus strength (0.5–1 mA) was titrated to obtain ~50% synaptic failures and was not changed during the experiment. Each condition was tested by delivering 20 stimulations at 1 Hz. Synapses with unstable postsynaptic potential amplitudes were rejected. We analyzed (i) synaptic efficacy defined as mean peak amplitude of all responses including failures, (ii) synaptic potency defined as mean peak amplitude of all successful responses, and (iii) probability of release or the ratio of the success versus total number of stimuli ($n = 20$). For analysis of paired-pulse facilitation, an electrode (FHC, CBARC75) was placed in the stratum radiatum at a distance of 100 µm from the patched CA1 neurons. eEPSPs were induced by delivering a 50- to 100-µA, 200-µs current. Analysis of data was performed with Clampfit 10.0 software (Axon Instruments) and SigmaPlot (Systat Software). For SNR analysis, eEPSPs were taken as signal, and sEPSPs were taken as noise. The integrated area of all the eEPSPs divided by the integrated area of all the sEPSPs within the same time period was used as SNR. The integrated area was calculated by the mean area multiplied by averaged frequency with Event Statistics collected in Clampfit 10.0 software. All results are reported as means ± SEM, and significance was determined by paired or unpaired $t$ tests or Tukey-Kramer post hoc multiple comparison tests.

For $Ca^{2+}$ imaging experiments, the slices were loaded with rhod-2 AM (4.5 µM, 1 hour). A custom-built microscope attached to Tsunami/Millennium laser (10 W, SpectraPhysics) and scanning box (FV 300, Olympus) with FluoView software and 40× objective (0.9 numerical aperture, Olympus) was used in all experiments (56). The excitation wavelength was fixed at 820 nm, whereas two-channel detection of emission was achieved by a 565-nm dichroic mirror (Chroma) and two external photomultiplier tubes. A 525/50 band-pass filter (Chroma) was used to detect GFP emission wavelength, and a 620/60 band-pass filter (Chroma) to detect rhod-2 signals. Relative changes in rhod-2 signaling were quantified with FluoView software. Time-lapse images of astrocytic $Ca^{2+}$ signaling were recorded every second. For $Ca^{2+}$ imaging experiments, the agonists were dissolved in aCSF containing fluorescein (1%) to visualize picospritzer-delivered solution. In experiments recording

GPCR-activated changes in K$^+$ or EPSPs, the agonists were delivered by perfusion for a period of 1 min unless otherwise noted. SBFI, tetraammonium salt was used to measure intracellular Na$^+$. SBFI was dissolved to 20 $\mu$M in intracellular solution and loaded into astrocytes through whole-cell patch clamp. The same parameters of two-photon imaging were used to image SBFI.

### In vivo K$^+$ recordings and Ca$^{2+}$ imaging

Adult mice (8 to 12 weeks old) were anesthetized with ketamine (60 to 80 mg kg$^{-1}$) and xylazine (10 to 20 mg kg$^{-1}$). Body temperature was monitored by a rectal probe and maintained at 37°C by a heating blanket (BS4, Harvard Apparatus). The mice were incubated and artificially ventilated with a small animal ventilator (SAAR-830, CWE) (56). Blood was taken through a femoral artery catheter, and $P$CO$_2$ (partial pressure of CO$_2$), $P$O$_2$ (partial pressure of O$_2$), and pH were analyzed in microsamples (Rapidlab 248, Bayer, sample size 40 ml). Experiments were completed only if physiological variables remained within normal limits. The normal limits for $P$CO$_2$ were set at 35 to 45 mmHg, $P$O$_2$ at 80 to 115 mmHg, and arterial blood pH at 7.35 to 7.45; body temperature was maintained at 37°C. A stainless steel frame with one opening was glued to the skull. A cranial borehole (~1.0 mm) was prepared below the hole in the metal plate over the parietal cortex, and the dura was carefully removed. The exposed cortex was loaded with rhod-2 AM (0.4 mM, 1 hour) (56). The cranial window was superfused with aCSF gassed with 5% CO$_2$ and 95% O$_2$ (57). A potassium-sensitive microelectrode was inserted 100 $\mu$m (cortical layer II) below the pial surface microelectrode. After a stable baseline recording was obtained, ATP (100 $\mu$M), FMRF (15 $\mu$M), or vehicle (aCSF) was superfused for 1 min. K$^+$-sensitive microelectrodes were calibrated before and after each recording. In selected experiments, the exposed cortex was loaded with rhod-2 AM (50 $\mu$M, 1 hour, 15 washes in aCSF). Time-lapse images of astrocytic Ca$^{2+}$ signaling were recorded every second by FluoView with the custom-built two-photon laser-scanning setup.

### Statistics

All histograms are expressed as means ± SEM. Student's *t* test or analysis of variance (ANOVA) with Bonferroni-Dunn post hoc tests was used, where normality of the data was assumed by Shapiro-Wilk's test. Otherwise, nonparametric Kruskal-Wallis test with Mann-Whitney pairwise test with Bonferroni-adjusted α level was used. For repeated measures, paired *t* test or repeated-measures ANOVA with Bonferroni-Dunn post hoc test was used, where normality and sphericity conditions were met.

## Supplementary Material

Refer to Web version on PubMed Central for supplementary material.

## Acknowledgments

## REFERENCES AND NOTES

1. Ransom CB, Ransom BR, Sontheimer H. Activity-dependent extracellular K$^+$ accumulation in rat optic nerve: The role of glial and axonal Na$^+$ pumps. J Physiol. 2000; 522(pt. 3):427–442. [PubMed: 10713967]

2. Evans SJ, Jones JV, Levi AJ. Reduction in external K causes increased action potential shortening in ventricular myocytes from the spontaneously hypertensive rat. J Hypertens. 1997; 15:659–666. [PubMed: 9218186]

3. Takahashi N, Kitamura K, Matsuo N, Mayford M, Kano M, Matsuki N, Ikegaya Y. Locally synchronized synaptic inputs. Science. 2012; 335:353–356. [PubMed: 22267814]

4. Bay V, Butt AM. Relationship between glial potassium regulation and axon excitability: A role for glial Kir4.1 channels. Glia. 2012; 60:651–660. [PubMed: 22290828]

5. Glitsch HG. Electrophysiology of the sodium-potassium-ATPase in cardiac cells. Physiol Rev. 2001; 81:1791–1826. [PubMed: 11581502]

6. Barres BA. The mystery and magic of glia: A perspective on their roles in health and disease. Neuron. 2008; 60:430–440. [PubMed: 18995817]

7. Clausen T. Regulation of active $Na^+$-$K^+$ transport in skeletal muscle. Physiol Rev. 1986; 66:542–580. [PubMed: 3016768]

8. Lüpfert C, Grell E, Pintschovius V, Apell HJ, Cornelius F, Clarke RJ. Rate limitation of the $Na^+$,$K^+$-ATPase pump cycle. Biophys J. 2001; 81:2069–2081. [PubMed: 11566779]

9. Pellerin L, Magistretti PJ. Glutamate uptake stimulates $Na^+$,$K^+$-ATPase activity in astrocytes via activation of a distinct subunit highly sensitive to ouabain. J Neurochem. 1997; 69:2132–2137. [PubMed: 9349559]

10. Stanimirovic DB, Ball R, Durkin JP. Stimulation of glutamate uptake and Na,K-ATPase activity in rat astrocytes exposed to ischemia-like insults. Glia. 1997; 19:123–134. [PubMed: 9034829]

11. Sontheimer H, Fernandez-Marques E, Ullrich N, Pappas CA, Waxman SG. Astrocyte Na+ channels are required for maintenance of $Na^+$/$K^+$-ATPase activity. J Neurosci. 1994; 14:2464–2475. [PubMed: 8182422]

12. Cornell-Bell AH, Finkbeiner SM, Cooper MS, Smith SJ. Glutamate induces calcium waves in cultured astrocytes: Long-range glial signaling. Science. 1990; 247:470–473. [PubMed: 1967852]

13. Nedergaard M. Direct signaling from astrocytes to neurons in cultures of mammalian brain cells. Science. 1994; 263:1768–1771. [PubMed: 8134839]

14. Parpura V, Basarsky TA, Liu F, Jeftinija K, Jeftinija S, Haydon PG. Glutamate-mediated astrocyte–neuron signalling. Nature. 1994; 369:744–747. [PubMed: 7911978]

15. Verkhratsky A, Parpura V, Rodriguez JJ. Where the thoughts dwell: The physiology of neuronal–glial "diffuse neural net". Brain Res Rev. 2011; 66:133–151. [PubMed: 20546785]

16. Gourine AV, Kasparov S. Astrocytes as brain interoceptors. Exp Physiol. 2011; 96:411–416. [PubMed: 21257664]

17. Walz W. Role of astrocytes in the clearance of excess extracellular potassium. Neurochem Int. 2000; 36:291–300. [PubMed: 10732996]

18. Giaume C. Astroglial wiring is adding complexity to neuroglial networking. Front Neuroenergetics. 2010; 2:129. [PubMed: 20922057]

19. Cotrina ML, Lin JH, Alves-Rodrigues A, Liu S, Li J, Azmi-Ghadimi H, Kang J, Naus CC, Nedergaard M. Connexins regulate calcium signaling by controlling ATP release. Proc Natl Acad Sci USA. 1998; 95:15735–15740. [PubMed: 9861039]

20. Bennett MV, Contreras JE, Bukauskas FF, Saez JC. New roles for astrocytes: Gap junction hemichannels have something to communicate. Trends Neurosci. 2003; 26:610–617. [PubMed: 14585601]

21. Agulhon C, Fiacco TA, McCarthy KD. Hippocampal short- and long-term plasticity are not modulated by astrocyte $Ca^{2+}$ signaling. Science. 2010; 327:1250–1254. [PubMed: 20203048]

22. Liu C, Hermann TE. Characterization of ionomycin as a calcium ionophore. J Biol Chem. 1978; 253:5892–5894. [PubMed: 28319]

23. Holtzclaw LA, Pandhit S, Bare DJ, Mignery GA, Russell JT. Astrocytes in adult rat brain express type 2 inositol 1,4,5-trisphosphate receptors. Glia. 2002; 39:69–84. [PubMed: 12112377]

24. Li X, Zima AV, Sheikh F, Blatter LA, Chen J. Endothelin-1–induced arrhythmogenic $Ca^{2+}$ signaling is abolished in atrial myocytes of inositol-1,4,5-trisphosphate(IP$_3$)–receptor type 2–deficient mice. Circ Res. 2005; 96:1274–1281. [PubMed: 15933266]

25. Hrabetová S, Chen KC, Masri D, Nicholson C. Water compartmentalization and spread of ischemic injury in thick-slice ischemia model. J Cereb Blood Flow Metab. 2002; 22:80–88. [PubMed: 11807397]

26. Rose CR, Ransom BR. Gap junctions equalize intracellular Na$^+$ concentration in astrocytes. Glia. 1997; 20:299–307. [PubMed: 9262234]

27. Rose CR, Ransom BR. Intracellular sodium homeostasis in rat hippocampal astrocytes. J Physiol. 1996; 491(Pt. 2):291–305. [PubMed: 8866855]

28. Ransom BR, Sontheimer H. The neurophysiology of glial cells. J Clin Neurophysiol. 1992; 9:224–251. [PubMed: 1375603]

29. Goldman WF, Yarowsky PJ, Juhaszova M, Krueger BK, Blaustein MP. Sodium/calcium exchange in rat cortical astrocytes. J Neurosci. 1994; 14:5834–5843. [PubMed: 7523629]

30. Kirischuk S, Kettenmann H, Verkhratsky A. Na$^+$/Ca$^{2+}$ exchanger modulates kainate-triggered Ca$^{2+}$ signaling in Bergmann glial cells in situ. FASEB J. 1997; 11:566–572. [PubMed: 9212080]

31. Matsuda T, Arakawa N, Takuma K, Kishida Y, Kawasaki Y, Sakaue M, Takahashi K, Takahashi T, Suzuki T, Ota T, Hamano-Takahashi A, Onishi M, Tanaka Y, Kameo K, Baba A. SEA0400, a novel and selective inhibitor of the Na$^+$-Ca$^{2+}$ exchanger, attenuates reperfusion injury in the in vitro and in vivo cerebral ischemic models. J Pharmacol Exp Ther. 2001; 298:249–256. [PubMed: 11408549]

32. Meral I, Hsu W, Hembrough FB. Digoxin- and monensin-induced changes of intracellular Ca$^{2+}$ concentration in isolated guinea-pig ventricular myocyte. J Vet Med A Physiol Pathol Clin Med. 2002; 49:329–333. [PubMed: 12227477]

33. Parekh AB, Putney JW Jr. Store-operated calcium channels. Physiol Rev. 2005; 85:757–810. [PubMed: 15788710]

34. Golovina VA. Visualization of localized store-operated calcium entry in mouse astrocytes. Close proximity to the endoplasmic reticulum. J Physiol. 2005; 564:737–749. [PubMed: 15731184]

35. Malarkey EB, Ni Y, Parpura V. Ca$^{2+}$ entry through TRPC1 channels contributes to intracellular Ca$^{2+}$ dynamics and consequent glutamate release from rat astrocytes. Glia. 2008; 56:821–835. [PubMed: 18338793]

36. Pivneva T, Haas B, Reyes-Haro D, Laube G, Veh RW, Nolte C, Skibo G, Kettenmann H. Store-operated Ca$^{2+}$ entry in astrocytes: Different spatial arrangement of endoplasmic reticulum explains functional diversity in vitro and in situ. Cell Calcium. 2008; 43:591–601. [PubMed: 18054077]

37. Torres A, Wang F, Xu Q, Fujita T, Dobrowolski R, Willecke K, Takano T, Nedergaard M. Extracellular Ca$^{2+}$ acts as a mediator of communication from neurons to glia. Sci Signal. 2012; 5:ra8. [PubMed: 22275221]

38. Kim SJ, Kim YS, Yuan JP, Petralia RS, Worley PF, Linden DJ. Activation of the TRPC1 cation channel by metabotropic glutamate receptor mGluR1. Nature. 2003; 426:285–291. [PubMed: 14614461]

39. Cheng XJ, Höög JO, Nairn AC, Greengard P, Aperia A. Regulation of rat Na$^+$-K$^+$-ATPase activity by PKC is modulated by state of phosphorylation of Ser-943 by PKA. Am J Physiol. 1997; 273:C1981–C1986. [PubMed: 9435504]

40. Poulsen H, Morth P, Egebjerg J, Nissen P. Phosphorylation of the Na$^+$,K-ATPase and the H$^+$,K$^+$-ATPase. FEBS Lett. 2010; 584:2589–2595. [PubMed: 20412804]

41. Gutnick MJ, Heinemann U, Lux HD. Stimulus induced and seizure related changes in extracellular potassium concentration in cat thalamus (VPL). Electroencephalogr Clin Neurophysiol. 1979; 47:329–344. [PubMed: 90603]

42. D'Ambrosio R, Gordon DS, Winn HR. Differential role of KIR channel and Na$^+$/K$^+$-pump in the regulation of extracellular K$^+$ in rat hippocampus. J Neurophysiol. 2002; 87:87–102. [PubMed: 11784732]

43. Meeks JP, Jiang X, Mennerick S. Action potential fidelity during normal and epileptiform activity in paired soma-axon recordings from rat hippocampus. J Physiol. 2005; 566:425–441. [PubMed: 15890699]

44. Meeks JP, Mennerick S. Selective effects of potassium elevations on glutamate signaling and action potential conduction in hippocampus. J Neurosci. 2004; 24:197–206. [PubMed: 14715952]

45. Browne SH, Kang J, Akk G, Chiang LW, Schulman H, Huguenard JR, Prince DA. Kinetic and pharmacological properties of GABA$_A$ receptors in single thalamic neurons and GABA$_A$ subunit expression. J Neurophysiol. 2001; 86:2312–2322. [PubMed: 11698521]

46. Chang SY, Zagha E, Kwon ES, Ozaita A, Bobik M, Martone ME, Ellisman MH, Heintz N, Rudy B. Distribution of Kv3.3 potassium channel subunits in distinct neuronal populations of mouse brain. J Comp Neurol. 2007; 502:953–972. [PubMed: 17444489]

47. Goldberg EM, Watanabe S, Chang SY, Joho RH, Huang ZJ, Leonard CS, Rudy B. Specific functions of synaptically localized potassium channels in synaptic transmission at the neocortical GABAergic fast-spiking cell synapse. J Neurosci. 2005; 25:5230–5235. [PubMed: 15917463]

48. Rudy B, McBain CJ. Kv3 channels: Voltage-gated K$^+$ channels designed for high-frequency repetitive firing. Trends Neurosci. 2001; 24:517–526. [PubMed: 11506885]

49. Svirskis G, Kotak V, Sanes DH, Rinzel J. Enhancement of signal-to-noise ratio and phase locking for small inputs by a low-threshold outward current in auditory neurons. J Neurosci. 2002; 22:11019–11025. [PubMed: 12486197]

50. Svirskis G, Dodla R, Rinzel J. Subthreshold outward currents enhance temporal integration in auditory neurons. Biol Cybern. 2003; 89:333–340. [PubMed: 14669013]

51. Freed MA, Liang Z. Reliability and frequency response of excitatory signals transmitted to different types of retinal ganglion cell. J Neurophysiol. 2010; 103:1508–1517. [PubMed: 20089819]

52. Pfrieger FW, Barres BA. Synaptic efficacy enhanced by glial cells in vitro. Science. 1997; 277:1684–1687. [PubMed: 9287225]

53. Perea G, Araque A. Astrocytes potentiate transmitter release at single hippocampal synapses. Science. 2007; 317:1083–1086. [PubMed: 17717185]

54. Meeks JP, Mennerick S. Astrocyte membrane responses and potassium accumulation during neuronal activity. Hippocampus. 2007; 17:1100–1108. [PubMed: 17853441]

55. Chever O, Djukic B, McCarthy KD, Amzica F. Implication of K$_{ir}$4.1 channel in excess potassium clearance: An in vivo study on anesthetized glial-conditional K$_{ir}$4.1 knock-out mice. J Neurosci. 2010; 30:15769–15777. [PubMed: 21106816]

56. Wang X, Lou N, Xu Q, Tian GF, Peng WG, Han X, Kang J, Takano T, Nedergaard M. Astrocytic Ca$^{2+}$ signaling evoked by sensory stimulation in vivo. Nat Neurosci. 2006; 9:816–823. [PubMed: 16699507]

57. Takano T, Tian GF, Peng W, Lou N, Lovatt D, Hansen AJ, Kasischke KA, Nedergaard M. Cortical spreading depression causes and coincides with tissue hypoxia. Nat Neurosci. 2007; 10:754–762. [PubMed: 17468748]

58. Hansen AJ. Effect of anoxia on ion distribution in the brain. Physiol Rev. 1985; 65:101–148. [PubMed: 3880896]

59. Bekar LK, He W, Nedergaard M. Locus coeruleus α-adrenergic–mediated activation of cortical astrocytes in vivo. Cereb Cortex. 2008; 18:2789–2795. [PubMed: 18372288]

60. Regan MR, Huang YH, Kim YS, Dykes-Hoberg MI, Jin L, Watkins AM, Bergles DE, Rothstein JD. Variations in promoter activity reveal a differential expression and physiology of glutamate transporters by glia in the developing and mature CNS. J Neurosci. 2007; 27:6607–6619. [PubMed: 17581948]

61. Syková E, Orkand RK. Extracellular potassium accumulation and transmission in frog spinal cord. Neuroscience. 1980; 5:1421–1428. [PubMed: 6250100]

62. Cochran SL. Cationic influences upon synaptic transmission at the hair cell-afferent fiber synapse of the frog. Neuroscience. 1995; 68:1147–1165. [PubMed: 8544989]

63. Orkand RK, Nicholls JG, Kuffler SW. Effect of nerve impulses on the membrane potential of glial cells in the central nervous system of amphibia. J Neurophysiol. 1966; 29:788–806. [PubMed: 5966435]

64. Newman EA, Frambach DA, Odette LL. Control of extracellular potassium levels by retinal glial cell K$^+$ siphoning. Science. 1984; 225:1174–1175. [PubMed: 6474173]

65. Han F, Bossuyt J, Martin JL, Despa S, Bers DM. Role of phospholemman phosphorylation sites in mediating kinase-dependent regulation of the Na$^+$-K$^+$-ATPase. Am J Physiol Cell Physiol. 2010; 299:C1363–C1369. [PubMed: 20861470]

66. Pannasch U, Vargova L, Reingruber J, Ezan P, Holcman D, Giaume C, Sykova E, Rouach N. Astroglial networks scale synaptic activity and plasticity. Proc Natl Acad Sci USA. 2011; 108:8467–8472. [PubMed: 21536893]

67. Geiger JR, Jonas P. Dynamic control of presynaptic $Ca^{2+}$ inflow by fast-inactivating $K^+$ channels in hippocampal mossy fiber boutons. Neuron. 2000; 28:927–939. [PubMed: 11163277]

68. Thio LL, Yamada KA. Differential presynaptic modulation of excitatory and inhibitory autaptic currents in cultured hippocampal neurons. Brain Res. 2004; 1012:22–28. [PubMed: 15158157]

69. Money TG, Rodgers CI, McGregor SM, Robertson RM. Loss of potassium homeostasis underlies hyperthermic conduction failure in control and preconditioned locusts. J Neurophysiol. 2009; 102:285–293. [PubMed: 19386751]

70. Lin JH, Weigel H, Cotrina ML, Liu S, Bueno E, Hansen AJ, Hansen TW, Goldman S, Nedergaard M. Gap-junction-mediated propagation and amplification of cell injury. Nat Neurosci. 1998; 1:494–500. [PubMed: 10196547]

71. Hounsgaard J, Nicholson C. Potassium accumulation around individual purkinje cells in cerebellar slices from the guineapig. J Physiol. 1983; 340:359–388. [PubMed: 6887054]

72. Nedergaard M, Hansen AJ. Characterization of cortical depolarizations evoked in focal cerebral ischemia. J Cereb Blood Flow Metab. 1993; 13:568–574. [PubMed: 8314912]

73. Messerli MA, Smith PJ. Construction, theory, and practical considerations for using self-referencing of $Ca^{2+}$-selective microelectrodes for monitoring extracellular $Ca^{2+}$ gradients. Methods Cell Biol. 2010; 99:91–111. [PubMed: 21035684]

74. Cotrina ML, Kang J, Lin JH, Bueno E, Hansen TW, He L, Liu Y, Nedergaard M. Astrocytic gap junctions remain open during ischemic conditions. J Neurosci. 1998; 18:2520–2537. [PubMed: 9502812]
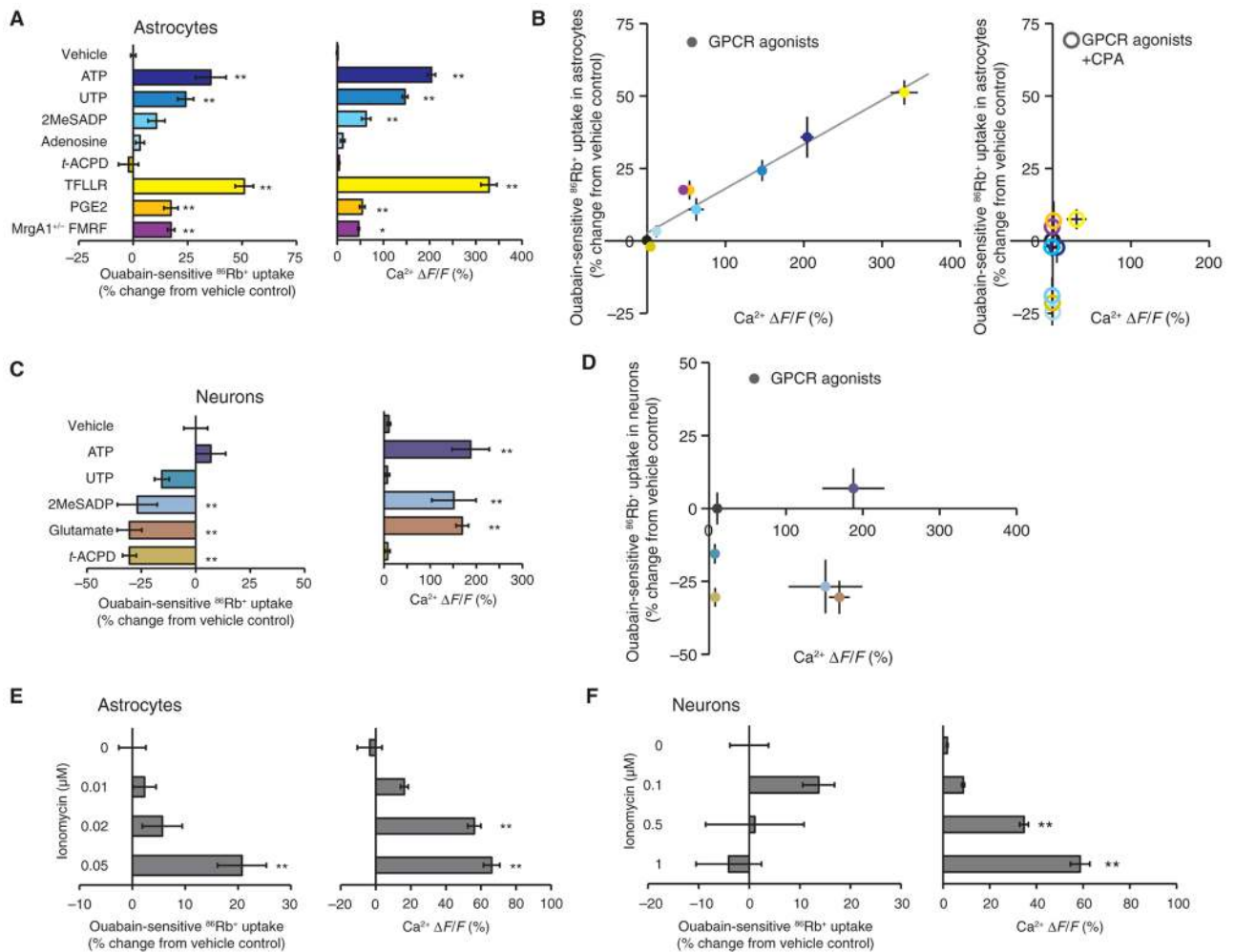
**Fig. 1.**
Receptor-mediated $Ca^{2+}$ signaling enhances astrocytic $K^+$ uptake in vitro. (**A**) The effect of GPCR agonists ATP (100 μM, $n = 27$), UTP (100 μM, $n = 39$), 2MeSADP (100 μM, $n = 8$), adenosine (100 μM, $n = 4$), t-ACPD (100 μM, $n = 8$), TFLLR-NH$_2$ (30 μM, $n = 37$), PGE$_2$ (50 μM, $n = 10$), or FMRF (15 μM in MrgA1$^{+/-}$ mice, $n = 12$) on ouabain-sensitive $^{86}Rb^+$ uptake in cultured astrocytes compared with vehicle (left). ** $P < 0.01$, Mann-Whitney $U$ test. Cytosolic $Ca^{2+}$ increases in response to the same agonists (right). The cultured astrocytes were loaded with the $Ca^{2+}$ indicator rhod-2 AM (4.5 μM). $n = 3$ to 5. * $P < 0.05$; ** $P < 0.01$, Bonferroni-Dunn test. (**B**) Relative increases in $^{86}Rb^+$ uptake plotted as a function of agonist-induced $Ca^{2+}$ increases in astrocytes ($y = 0.153x + 2.90$, $r^2 = 0.94$). CPA (20 μM, right) eliminated agonist-induced enhancement of $^{86}Rb^+$ uptake ($n = 9$). (**C**) The effect of ATP, UTP, 2MeSADP, glutamate, and t-ACPD (all 100 μM, $n = 4$ to 8) on $^{86}Rb^+$ uptake in cultured neurons (left) with corresponding agonist-evoked increases in $Ca^{2+}$ (right). Cultured neurons were loaded with the $Ca^{2+}$ indicator rhod-2 AM (4.5 μM). $n = 3$ to 5. ** $P < 0.01$, Bonferroni-Dunn test. (**D**) Relative increases in $^{86}Rb^+$ uptake plotted as a function of agonist-induced $Ca^{2+}$ increases in neurons. (**E** and **F**) Effect of the $Ca^{2+}$ ionophore, ionomycin, on $^{86}Rb^+$ uptake and $Ca^{2+}$ increases in astrocytes (E) ($n = 4$ to 12, ** $P < 0.01$, Bonferroni-Dunn test) and neurons (F) ($n = 4$ to 8, ** $P < 0.01$, Bonferroni-Dunn test).
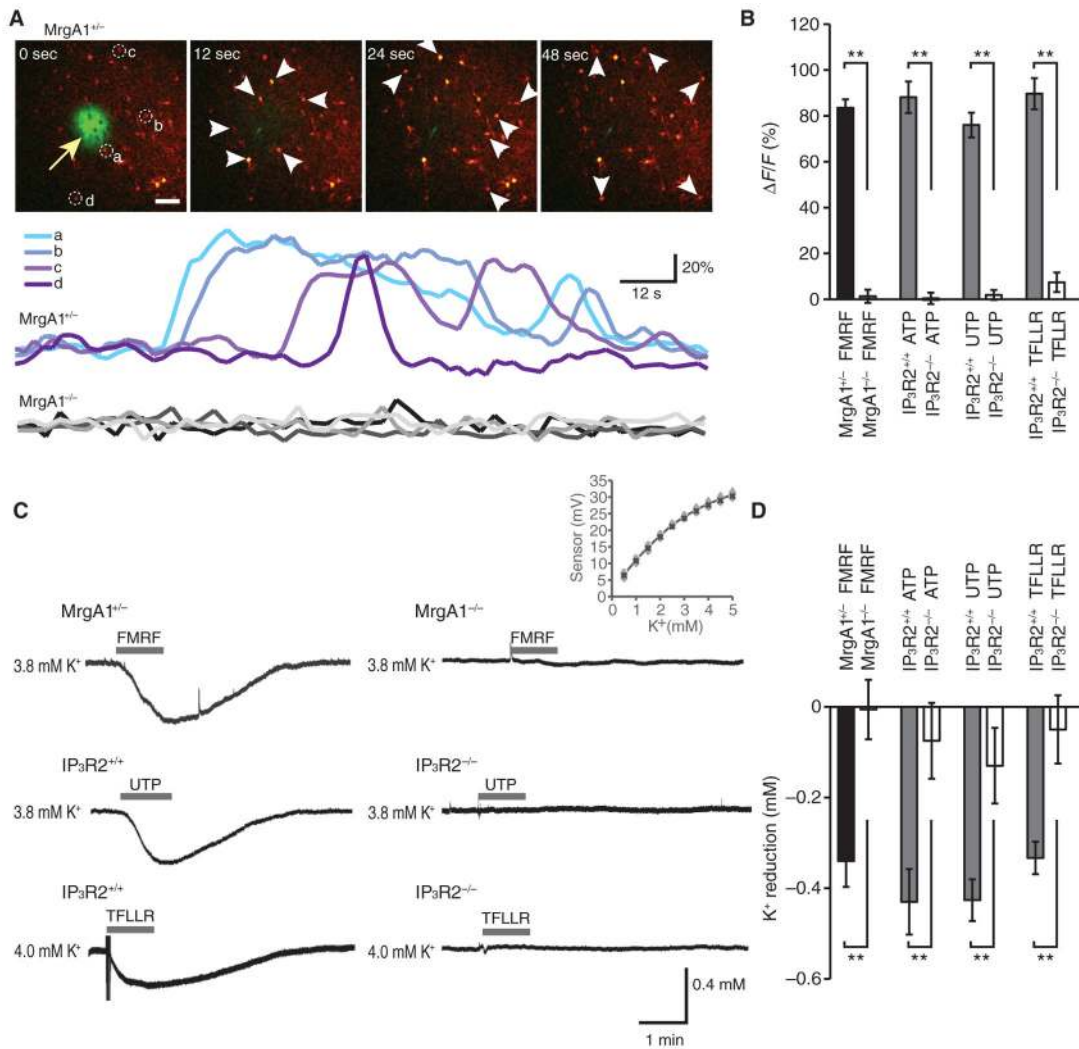
**Fig. 2.**
Receptor-mediated astrocytic $Ca^{2+}$ signaling enhances $K^+$ uptake in hippocampal slices. (**A**) Time-lapse images of FMRF-induced increases in $Ca^{2+}$ in a hippocampal slice prepared from a MrgA1$^{+/-}$ mouse loaded with rhod-2 AM (4.5 μM). The pipette solution contained, in addition to FMRF (15 μM), fluorescein isothiocyanate (FITC)–dextran (1%, 10 kD) to visualize delivery of agonist (arrow). Colored traces indicate relative changes in rhod-2 signals of astrocytes (a to d) labeled in the first panel, whereas gray traces at the bottom show the effect of FMRF in a MrgA1$^{-/-}$littermate. Scale bar, 50 μm. (**B**) Bar graph comparing relative increases in $Ca^{2+}$ (rhod-2 signal, $\Delta F/F$) in astrocytes in MrgA1$^{+/-}$ and MrgA1$^{-/-}$ mice ($n = 3$ to 6 slices) and the effects of agonist exposure, ATP (100 μM), UTP (100 μM), and TFLLR-NH$_2$ (30 μM), in slices prepared from wild-type and IP$_3$R2$^{-/-}$ mice. **$P < 0.01$, $t$ test. (**C**) Recordings of extracellular $K^+$ concentration in hippocampal slices exposed to FMRF, UTP, or TFLLR-NH$_2$. The slices were prepared from wild-type (IP$_3$R2$^{+/+}$), IP$_3$R2$^{-/-}$, or MrgA1$^{+/-}$ and MrgA1$^{-/-}$ mice as indicated. Inset: average calibration of $K^+$-sensitive microelectrodes. (**D**) Bar graph comparing relative changes in extracellular $K^+$ in hippocampal slices exposed to ATP ($n = 6$ for both IP$_3$R2$^{+/+}$ and IP$_3$R2$^{-/-}$), UTP ($n = 6$ for both IP$_3$R2$^{+/+}$ and IP$_3$R2$^{-/-}$), and TFLLR-NH$_2$ ($n = 8$ for IP$_3$R2$^{+/+}$ and $n = 5$ for IP$_3$R2$^{-/-}$) in slices prepared from IP$_3$R2$^{+/+}$ and IP$_3$R2$^{-/-}$ mice, as

well as exposure to FMRF in slices prepared from MrgA1$^{+/-}$ ($n$ = 6) and MrgA1$^{-/-}$ mice ($n$ = 5). **$P$ < 0.01, $t$ test.
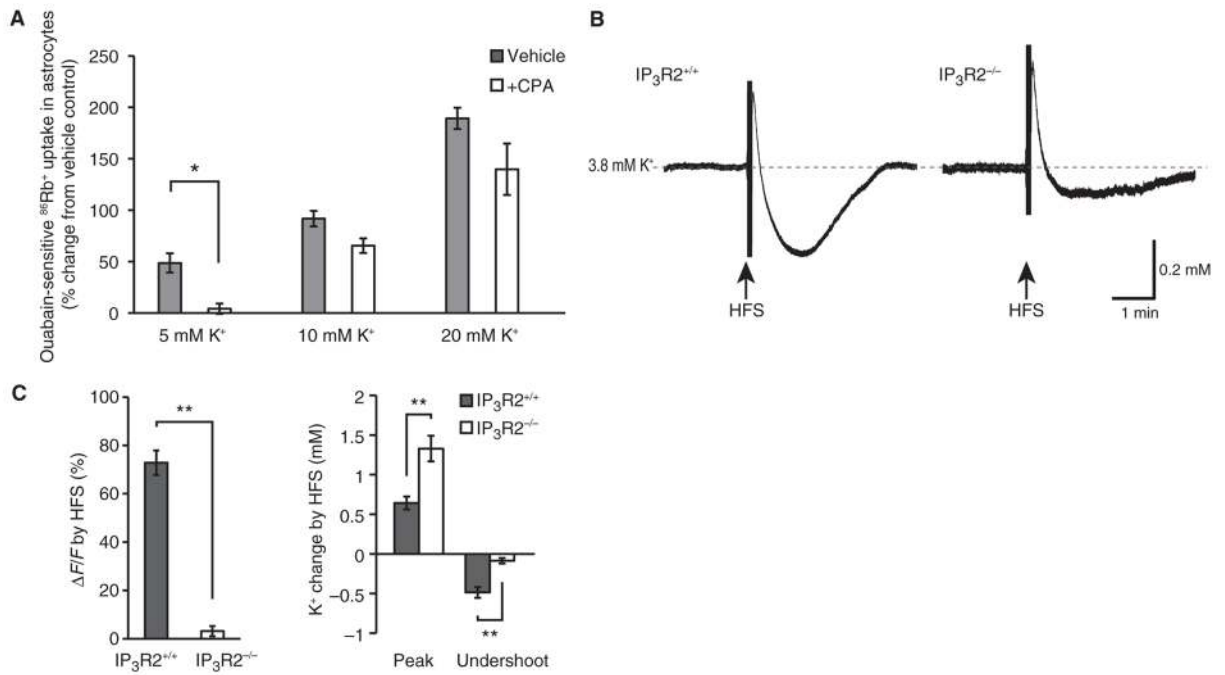
**Fig. 3.**
Astrocytic calcium transients contribute to $K^+$ clearance in response to moderate, but not pathophysiological, changes in extracellular $K^+$ in cultured astrocytes and in hippocampal slices. (**A**) Bar graph illustrating the calcium dependence of ouabain-sensitive $^{86}Rb^+$ uptake in cultured astrocytes to physiological and pathophysiological changes in extracellular $K^+$ concentration ($n = 4$ slices). $*P < 0.05$, $t$ test. (**B**) HFS-induced changes in extracellular $K^+$ in wild-type ($IP_3R2^{+/+}$) and $IP_3R2^{-/-}$ mice. Dashed line indicates baseline $K^+$ concentration. (**C**) Bar graphs comparing relative increase in $Ca^{2+}$ (rhod-2 signal, $n = 12$ slices, $\Delta F/F$, left panel) and changes in extracellular $K^+$ (peak increase and undershoot) in $IP_3R2^{+/+}$ and $IP_3R2^{-/-}$ mice (right panel, $n = 7$ slices). $**P < 0.01$, $t$ test.
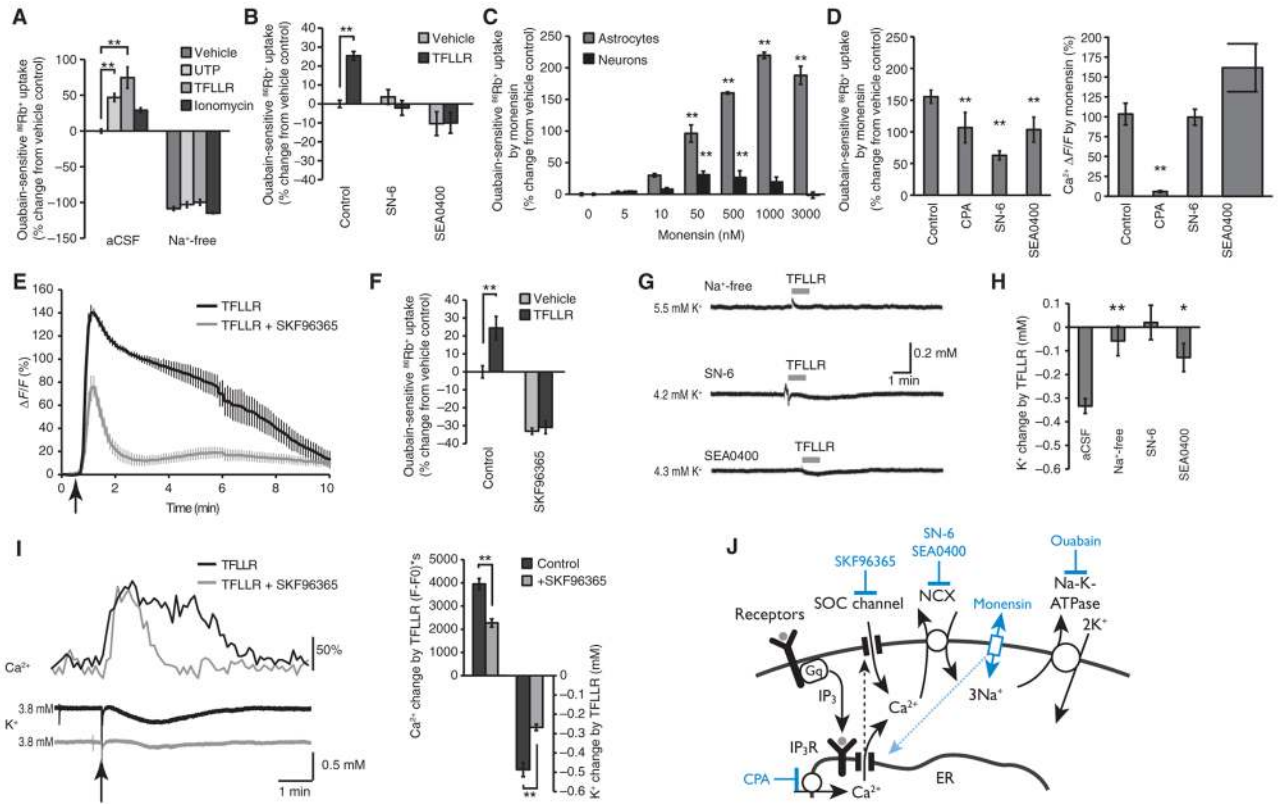
**Fig. 4.**
Agonist-induced astrocytic $Ca^{2+}$ signaling drives $K^+$ uptake by increasing $Na^+$ availability in cultured astrocytes and in hippocampal slices. (**A**) Effects of replacement of extracellular $Na^+$ on $^{86}Rb^+$ uptake under baseline conditions and in response to UTP (100 $\mu$M, $n = 7$), TFLLR-$NH_2$ (30 $\mu$M, $n = 7$), or ionomycin (0.05 $\mu$M) in cultured astrocytes. $n = 3$ to 7 wells. \*\*$P < 0.01$, Mann-Whitney $U$ test. (**B**) Effects of the $Na^+,Ca^{2+}$ exchange inhibitors, SN-6 (10 $\mu$M) and SEA0400 (10 $\mu$M) on baseline, and agonist (30 $\mu$M TFLLR-$NH_2$)–induced $^{86}Rb^+$ uptake in cultured astrocytes. $n = 3$ to 6 wells. \*\*$P < 0.01$, Mann-Whitney $U$ test. (**C**) Effects of increasing concentration of monensin, a $Na^+$ ionophore, on $^{86}Rb^+$ uptake in cultured astrocytes and neurons. $n = 4$ to 8 wells. \*\*$P < 0.01$ compared to before, Bonferroni-Dunn test. (**D**) Effects of CPA (20 $\mu$M), SN-6 (10 $\mu$M), and SEA0400 (10 $\mu$M) on monensin (3 $\mu$M)–induced $^{86}Rb^+$ uptake in cultured astrocytes ($n = 6$ to 15 wells; \*\*$P < 0.01$ compared to before, Bonferroni-Dunn test) with corresponding agonist-evoked $Ca^{2+}$ increases (right panel; $n = 4$ wells, \*\*$P < 0.01$ compared to before, Bonferroni-Dunn test). (**E** and **F**) Store-operated calcium channel blocker SKF96365 (25 $\mu$M) reduced both the increase in cytosolic $Ca^{2+}$ evoked by ATP ($n = 4$ wells) and the $^{86}Rb^+$ uptake by 30 $\mu$M TFLLR-$NH_2$ ($n = 4$ wells) in cultured astrocytes. Arrow indicates the time ATP was applied to the cells. \*\*$P < 0.01$, $t$ test. (**G**) Effects of replacing extracellular $Na^+$ with $NMDG^+$, or addition of NCX blockers SN-6 (10 $\mu$M) and SEA0400 (15 $\mu$M) on TFLLR-$NH_2$–induced (100 $\mu$M) changes in extracellular $K^+$ concentration in hippocampal slices. (**H**) Comparison of TFLLR-$NH_2$–induced changes in extracellular K+ under Na+-free ($n = 6$) and control conditions in the presence of SN-6 ($n = 5$) or SEA0400 ($n = 5$) in hippocampal slices. \*$P < 0.05$; \*\*$P < 0.01$, Bonferroni-Dunn test. (**I**) Typical trace illustrating $Ca^{2+}$ waves and $K^+$ recordings activated by TFLLR-$NH_2$ (30 $\mu$M) in hippocampal slices with or without SKF96365 (25 $\mu$M) with corresponding bar graphs compared on the right. $n = 8$ to 13, \*\*$P$

$< 0.01$, *t* test. (**J**) Diagram of proposed pathways involved in agonist-induced $K^+$ uptake in astrocytes.
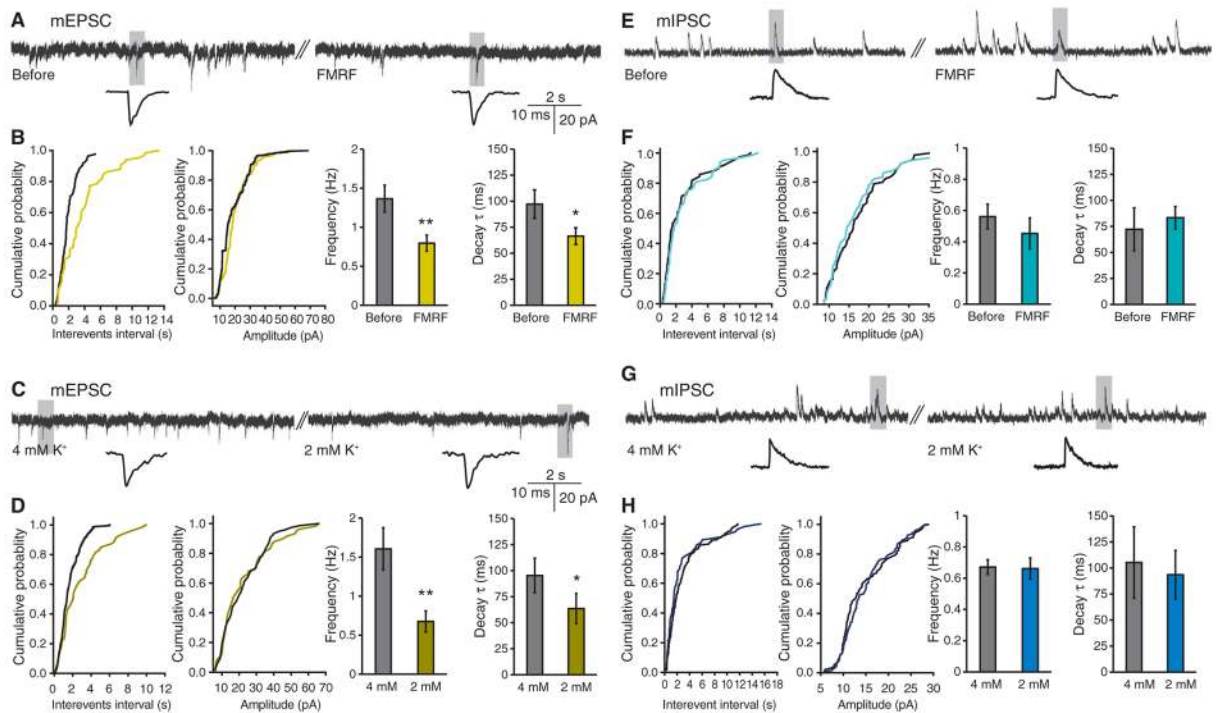
**Fig. 5.**
Astrocytic $Ca^{2+}$ signaling decreases mEPSC frequency but not mIPSC frequency in hippocampal slices. (**A**) Representative recordings of mEPSCs before and after superfusion of FMRF (15 μM) in slices prepared from MrgA1$^{+/-}$ mice. (**B**) Cumulative analysis of the inter-event interval and amplitude of mEPSCs in a 1-min representative recording before and during application of FMRF. Bar graphs compare frequency and time constant of decay (τ). $n = 9$ slices. *$P < 0.05$; **$P < 0.01$ compared to before FMRF treatment, paired $t$ test. (**C**) Representative recordings of mEPSCs when bath $K^+$ concentration was decreased from 4 to 2 mM; shaded area is shown below at extended time scale. (**D**) Cumulative analyses of the inter-event interval and amplitude of mEPSCs. Bar graphs compare frequency and decay τ of mEPSCs. $n = 8$ slices. *$P < 0.05$; **$P < 0.01$ compared to 4 mM $K^+$, paired $t$ test. (**E**) Representative recordings of mIPSCs before and after perfusion of FMRF in slices prepared from MrgA1$^{+/-}$ mice. (**F**) Cumulative analyses of the inter-event interval and amplitude of mIPSCs from representative traces. Comparison of the effect of FMRF on frequency and decay τ ($n = 7$ slices, paired $t$ test). (**G**) Representative recordings of mIPSCs when bath $K^+$ concentration was decreased from 4 to 2 mM. (**H**) Cumulative analyses of the inter-event interval and amplitude of mIPSCs. Histograms compare frequency and decay τ of mIPSCs ($n = 7$ slices, paired $t$ test).
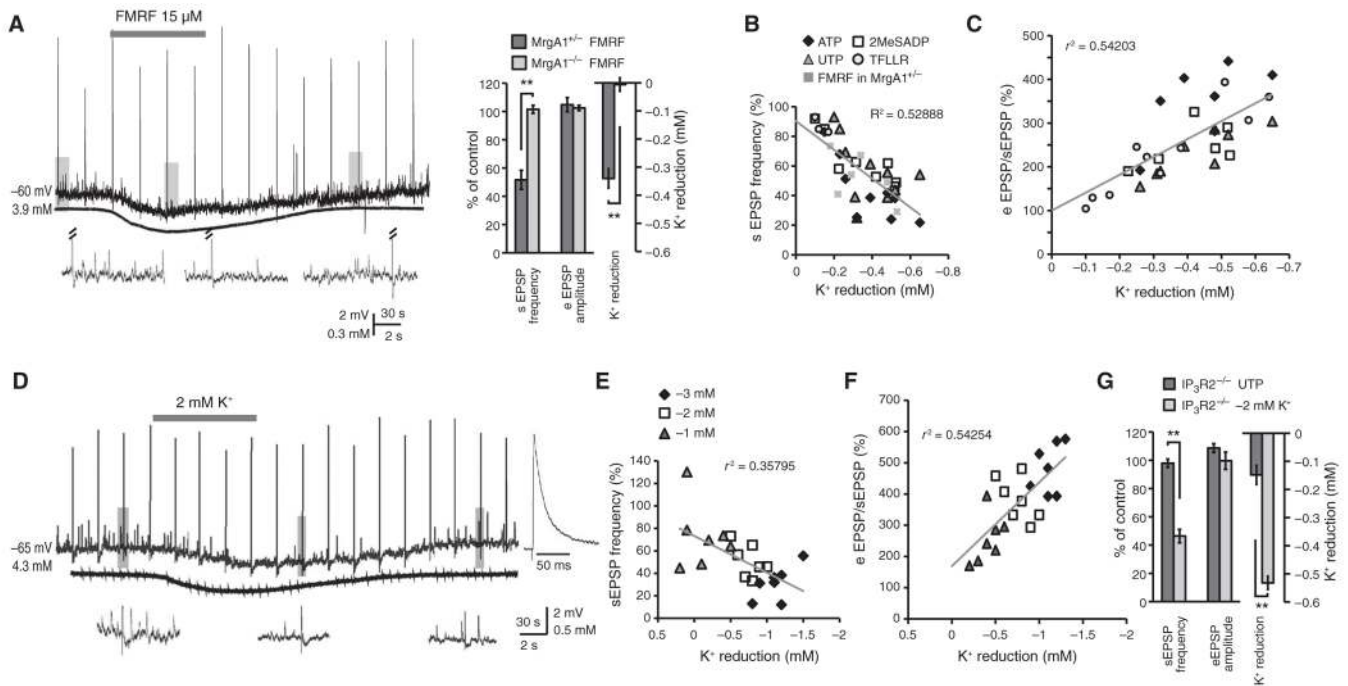
**Fig. 6.**
Suppression of spontaneous excitatory activity in hippocampal slices in response to $Ca^{2+}$ signaling in astrocytes. (**A**) Left: whole-cell recording of CA1 pyramidal neurons combined with measurements of extracellular $K^+$ in a hippocampal slice. Representative recording of sEPSPs and eEPSPs in a CA1 hippocampal neuron in response to FMRF (15 μM) in a slice prepared from a MrgA1$^{+/-}$ mouse. Enlarged time scales of EPSPs for the indicated periods are shown at the bottom. Right: bar graph comparing the effect of FMRF on the frequency of sEPSPs and amplitude of eEPSPs in CA1 neurons in slices prepared from MrgA1$^{+/-}$ ($n =$ 6 slices) or MrgA1$^{-/-}$($n = 5$ slices) mice. Concomitant changes in extracellular $K^+$ are also shown. $**P < 0.01$, $t$ test. (**B**) The frequency of sEPSPs plotted as a function of changes in extracellular $K^+$ concentration in response to agonist exposure (ATP, 2MeSADP, UTP, TFLLR-NH$_2$, or FMRF) in MrgA1$^{+/-}$ mice. (**C**) The ratio of integrated areas of eEPSPs and sEPSPs increased as a direct function of the decrease in extracellular $K^+$ induced by agonist exposure ($r^2 = 0.54$). (**D**) Representative recording of sEPSPs together with eEPSPs from five CA1 hippocampal slices when $K^+$ in the bath solution was transiently reduced from 4 to 2 mM. Enlarged time scales of the indicated periods are shown at the bottom. Trace on the right shows enlarged time scale for eEPSP recorded in 4 mM $K^+$. (**E**) Relative changes in the frequency of sEPSP plotted as a function of the decrease in extracellular $K^+$ induced by lowering bath $K^+$ concentration. (**F**) The ratio of integrated area of eEPSPs and sEPSPs during the same time period increases as a direct function of lowering extracellular $K^+$ ($r^2 = 0.54$). (**G**) Effects of UTP or reduction of extracellular $K^+$ (from 4 to 2 mM) on the frequency of sEPSPs and amplitude of eEPSPs in CA1 hippocampal neurons in slices prepared from IP$_3$R$_2$−/− mice ($n = 5$ slices). Concomitant changes in extracellular $K^+$ are also plotted. $**P < 0.01$, $t$ test.
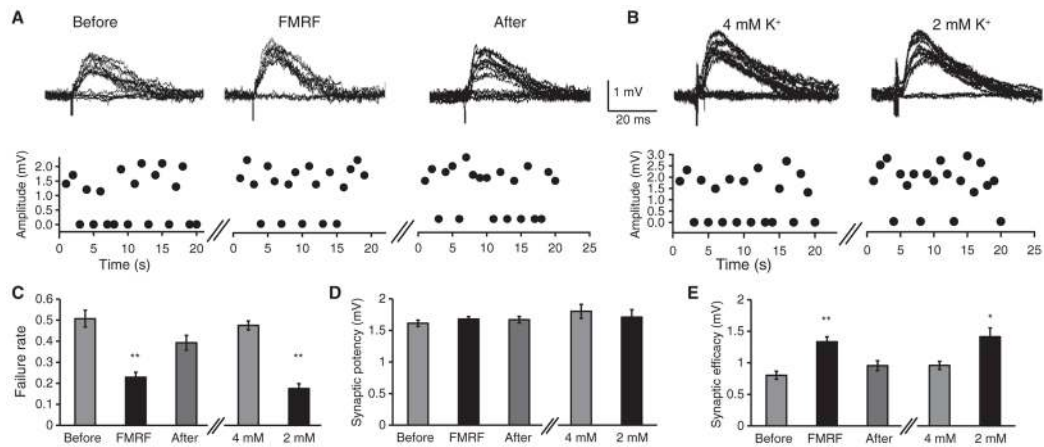
**Fig. 7.**
Astrocytic $Ca^{2+}$ signaling increases synaptic efficacy in hippocampal slices. (**A**) Failure rate from a representative recording in response to minimal stimulation before, during, or after application of FMRF in MrgA1$^{+/-}$ mice. Traces show eEPSP amplitude. (**B**) Failure rate to minimal stimulation in 4 or 2 mM K$^+$ perfusate. (**C**) Comparison of the effects of FMRF ($n$ = 7 slices, **$P < 0.01$ compared to before FMRF treatment, Bonferroni-Dunn test) and extracellular K$^+$ ($n$ = 8 slices, **$P < 0.01$ compared to 4 mM K$^+$, paired $t$ test) on failure rate. (**D** and **E**) Effects of FMRF and K$^+$ on (D) synaptic potency (mean amplitude of EPSP successes) and (E) synaptic efficacy (mean amplitude of all trials). $n$ = 7 slices, repeated-measures ANOVA for FMRF; $n$ = 8 slices, paired $t$ test for K$^+$, **$P < 0.01$, *$P < 0.05$).
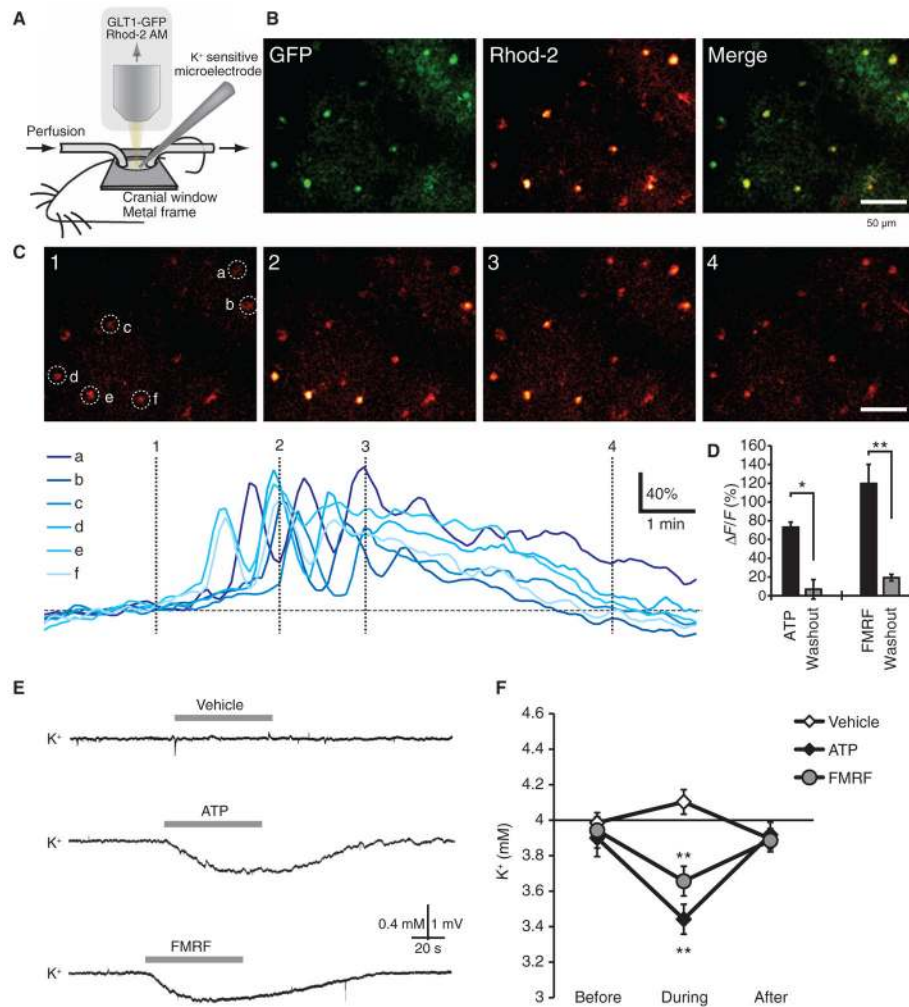
**Fig. 8.**
Agonist-induced increases in astrocytic $Ca^{2+}$ reduce extracellular $K^+$ concentration in vivo.
(**A**) Experimental setup for in vivo recordings. (**B**) Glt1-eGFP reporter mouse loaded with
the $Ca^{2+}$ indicator rhod-2 AM. Rhod-2 only–labeled eGFP$^+$ astrocytes. (**C**) Time-lapse
images of ATP (100 $\mu$M)–evoked increases in $Ca^{2+}$ in astrocytes located 95 $\mu$m below the
pial surface. Colored traces indicate relative changes in rhod-2 signals of astrocytes (a to f)
labeled in the first panel. (**D**) Comparison of ATP (100 $\mu$M)– and FMRF (15 $\mu$M)–induced
increases in rhod-2 signal ($\Delta F/F$). $n = 4$ to 5 mice. *$P < 0.05$; **$P < 0.01$, paired $t$ test. (**E**)
Representative recordings of extracellular $K^+$ concentration in mouse cortex exposed to
vehicle (aCSF), ATP (100 $\mu$M), or FMRF (15 $\mu$M). (**F**) Graph comparing the effects of
vehicle, ATP, and FMRF on extracellular $K^+$. All recordings were obtained 100 $\mu$m below
the cortical surface. $n = 7$ mice. **$P < 0.01$, Bonferroni-Dunn test compared to baseline.